

This discussion paper is/has been under review for the journal Atmospheric Chemistry and Physics (ACP). Please refer to the corresponding final paper in ACP if available.

# The CarboCount CH sites: characterization of a dense greenhouse gas observation network

B. Oney<sup>1,2</sup>, S. Henne<sup>1</sup>, N. Gruber<sup>2,3</sup>, M. Leuenberger<sup>4</sup>, I. Bamberger<sup>5,\*</sup>,  
W. Eugster<sup>5</sup>, and D. Brunner<sup>1,2</sup>

<sup>1</sup>Empa, Lab. for Air Pollution/Environmental Technology, Dübendorf, Switzerland

<sup>2</sup>ETH Zurich, Center for Climate Systems Modeling, Zurich, Switzerland

<sup>3</sup>ETH Zurich, Inst. of Biogeochemistry und Pollutant Dynamics, Zurich, Switzerland

<sup>4</sup>Univ. of Bern, Physics Inst., Climate and Environmental Division, and Oeschger Centre for Climate Change Research, Bern, Switzerland

<sup>5</sup>ETH Zurich, Inst. of Agricultural Sciences, Zurich, Switzerland

\* now at: Karlsruhe Institute of Technology KIT Institute of Meteorology and Climate Research Atmospheric Environmental Research (IMK-IFU) Kreuzeckbahnstraße 19, 82467 Garmisch-Partenkirchen, Germany

Received: 24 January 2015 – Accepted: 25 March 2015 – Published: 4 May 2015

Correspondence to: D. Brunner (dominik.brunner@empa.ch)

Published by Copernicus Publications on behalf of the European Geosciences Union.

Title Page

Abstract

Introduction

Conclusions

References

Tables

Figures

◀

▶

◀

▶

Back

Close

Full Screen / Esc

Printer-friendly Version

Interactive Discussion



## Abstract

We describe a new rural network of four densely placed (< 100 km apart), continuous atmospheric carbon ( $\text{CO}_2$ ,  $\text{CH}_4$ , and CO) measurement sites in north-central Switzerland and analyze their suitability for regional-scale (~ 100 to 500 km) carbon flux studies. We characterize each site by analyzing surrounding land cover, observed local meteorology, and sensitivity to surface fluxes, as simulated with the Lagrangian particle dispersion model FLEXPART-COSMO.

The Beromünster measurements are made on a tall tower (212 m) located on a gentle hill. At Beromünster, regional  $\text{CO}_2$  signals (measurement minus background) vary diurnally from -4 to +4 ppmv on average, and are simulated to come from nearly the entire Swiss Plateau, where 50 % of surface influence is simulated to be within 130 to 260 km distance. The Früebüel site measurements are made 4 m above ground on the flank of a gently sloping mountain. Nearby (< 50 km) pasture and forest fluxes exert the most simulated surface influence, except during convective summertime days when the site is mainly influenced by the eastern Swiss Plateau, which results in summertime regional  $\text{CO}_2$  signals varying diurnally from -5 to +12 ppmv and elevated summer daytime  $\text{CH}_4$  signals (+30 ppbv above other sites). The Gimmiz site measurements are made on a small tower (32 m) in flat terrain. Here, strong summertime regional signals (-5 to +60 ppmv  $\text{CO}_2$ ) stem from large, nearby (< 50 km) crop and anthropogenic fluxes of the Seeland region, except during warm or windy days when simulated surface influence is of regional scale (< 250 km). The Lägern-Hochwacht measurements are made on a small tower (32 m) on top of the steep Lägern crest, where simulated surface influence is typically of regional scale (130 to 300 km) causing summertime regional signals to vary from -5 to +8 ppmv  $\text{CO}_2$ . Here, considerable anthropogenic influence from the nearby industrialized region near Zurich cause the average wintertime regional  $\text{CO}_2$  signals to be 5 ppmv above the regional signals simultaneously measured at Früebüel site.

ACPD

15, 12911–12956, 2015

## Greenhouse gas observation network characterization

B. Oney et al.

|  |                              |
|--|------------------------------|
| <a href="#">Title Page</a>               |                              |
| <a href="#">Abstract</a>                 | <a href="#">Introduction</a> |
| <a href="#">Conclusions</a>              | <a href="#">References</a>   |
| <a href="#">Tables</a>                   | <a href="#">Figures</a>      |
| <a href="#">◀</a>                        | <a href="#">▶</a>            |
| <a href="#">◀</a>                        | <a href="#">▶</a>            |
| <a href="#">Back</a>                     | <a href="#">Close</a>        |
| <a href="#">Full Screen / Esc</a>        |                              |
| <a href="#">Printer-friendly Version</a> |                              |
| <a href="#">Interactive Discussion</a>   |                              |



## 10 1 Introduction

The exchange of carbon dioxide ( $\text{CO}_2$ ) with the terrestrial biosphere dominates the observed year-to-year variability in the global carbon sinks (Battle et al., 2000; Sarmiento et al., 2010; Le Quéré et al., 2010) even though land surfaces cover only 30 % of the Earth's surface area. Yet, our ability to quantify this variability in the net terrestrial carbon flux directly from observations has remained limited (Ciais et al., 2014). As a result, in most attempts to determine the global carbon budget, the net terrestrial carbon flux is estimated as the difference between the observed atmospheric carbon growth rate, and the sum of oceanic and anthropogenic carbon fluxes (Sarmiento et al., 2010; Le Quéré et al., 2013). Additionally, the lack of understanding of the feedbacks between 15 climate change and the terrestrial biosphere translates into one of the greatest uncertainties of future climate change projections (Heimann and Reichstein, 2008). An important step toward the reduction of this uncertainty is a better understanding of how the terrestrial biosphere responds to climatic fluctuations and trends. As the processes governing this response are inherently local to regional, this requires the determination 20 of terrestrial carbon fluxes at high spatial resolution (Gerbig et al., 2009).

The currently employed methods to determine terrestrial carbon fluxes from observations include global networks of background  $\text{CO}_2$  measurements (Tans et al., 1996)



that permit the determination of fluxes at continental scales (Gerbig et al., 2003a), and eddy covariance-based surface flux measurements that have a small-scale ( $\sim 1$  km) footprint (Baldocchi et al., 2001). This leaves an obvious gap at intermediate scales (10 to 10 000 km), which clearly needs to be filled in order to reliably determine the terrestrial carbon budget (Ciais et al., 2014). The establishment of the North American (Bakwin et al., 1998) and European (<http://www.chiotto.org/>; Vermeulen et al., 2004) tall tower networks represented a big step in this direction, but the high spatial heterogeneity of land cover and the correspondingly large variations in the CO<sub>2</sub> fluxes require even denser observation networks, especially in order to target regional scale (< 1000 km) carbon fluxes (Dolman et al., 2009; Lauvaux et al., 2012). The spatial density of a measurement network required to resolve the spatial distribution of carbon fluxes is dependent on the region of interest and the corresponding carbon flux signatures, and largely remains an open question (Groenendijk et al., 2011; Lauvaux et al., 2012).

Short-term measurement campaigns, such as the Large-Scale Biosphere-Atmosphere Experiment in Amazonia (Andreae et al., 2002), the CO<sub>2</sub> Budget and Rectification Airborne study (Gerbig et al., 2003b), and the CarboEurope Regional Experiment Strategy study (Dolman et al., 2006), have demonstrated the value of regional scale (< 1000 km) datasets, but lacked the temporal coverage for the calculation of annual carbon budgets and the investigation of seasonal carbon flux variation. The Mid-Continent Intensive (MCI) measurement campaign attempted to oversample the US upper midwest over a longer period of time (2007–2009; Miles et al., 2012), but even with an average distance of approximately 188 km between eight towers, Lauvaux et al. (2012) found that the spatial density of the measurement network was insufficient to consistently retrieve the spatial distribution of carbon fluxes.

The CarboCount CH project (<http://www.carbocount.ch>) was designed to overcome some of these limitations. It aims to quantify terrestrial carbon fluxes at high temporal and spatial resolution for multiple years through a combination of greenhouse gas concentration measurements and high-resolution atmospheric transport model-

[Title Page](#)[Abstract](#)[Introduction](#)[Conclusions](#)[References](#)[Tables](#)[Figures](#)[|◀](#)[▶|](#)[◀](#)[▶](#)[Back](#)[Close](#)[Full Screen / Esc](#)[Printer-friendly Version](#)[Interactive Discussion](#)

ing. Four greenhouse gas measurement sites have been established in the Swiss Plateau (Fig. 1), which is a densely settled, partly flat and hilly region between the Alps and Jura mountains approximately 50 km by 200 km in size with an average altitude of  $\sim 450$  m a.s.l. The measurement sites are located in rural areas and the average distance between sites is 85 km. The main goal of the CarboCount CH project is to better understand surface fluxes of carbon, which for carbon dioxide ( $\text{CO}_2$ ) mainly consist of anthropogenic emissions and biospheric activity, and for methane ( $\text{CH}_4$ ) mainly ( $\sim 80\%$ ) consist of agricultural emissions (Hiller et al., 2014).

The CarboCount CH measurement network includes measurement sites in complex terrain, which warrants the use of high resolution transport models (Pillai et al., 2011). A measurement site's local environment, especially the topography and land cover within  $< 3$  km distance, exerts influence on the local meteorology and thereby largely determines the local surface influence on observed trace gas concentrations (Vesala et al., 2008). Currently, most surface flux estimation studies usually use only afternoon measurements when the ABL is thickest and well-mixed to reduce the sensitivity to errors in the representation of the ABL by the underlying atmospheric transport models (Gerbig et al., 2009; Pillai et al., 2012; Kretschmer et al., 2014). Owing to the requirement of high resolution transport models to represent the winds in complex terrain, many inverse modeling studies do not use trace gas concentration measurements from mountain sites.

The purpose of this study is to characterize the CarboCount CH observation network. We describe the local environment of each of the four measurement sites and investigate how much the local environment influences meteorology and greenhouse gas measurements. Furthermore, we assess the sensitivity of each measurement site to regional surface fluxes with the Lagrangian particle dispersion model FLEXPART-COSMO. Due to the dependence on the employed atmospheric transport model to represent local and regional surface influence, we evaluate simulated meteorology in order to uncover possible transport simulation problems. Thus, we assess the informa-

|  |                              |
|--|------------------------------|
| <a href="#">Title Page</a>               |                              |
| <a href="#">Abstract</a>                 | <a href="#">Introduction</a> |
| <a href="#">Conclusions</a>              | <a href="#">References</a>   |
| <a href="#">Tables</a>                   | <a href="#">Figures</a>      |
| <a href="#"></a>                         | <a href="#"></a>             |
| <a href="#"></a>                         | <a href="#"></a>             |
| <a href="#">Full Screen / Esc</a>        |                              |
| <a href="#">Printer-friendly Version</a> |                              |
| <a href="#">Interactive Discussion</a>   |                              |



tion content of each site's measurements and establish potential guidelines for future transport and inverse modeling studies.

## 2 Data and methods

### 2.1 Measurement data

- The four measurement sites of the CarboCount CH network (Fig. 1 and Table 1) were equipped with PICARRO (Santa Clara, California, USA) cavity ring-down spectrometers for greenhouse gases measurements (Crosson, 2008; Rella et al., 2013). Additionally, meteorological variables including horizontal wind, humidity, dewpoint, and temperature were measured at all four sites. At Beromünster (BEO), air was sampled from five different heights (212, 132, 72, 45, and 12 m a.g.l.), and carbon dioxide ( $\text{CO}_2$ ), methane ( $\text{CH}_4$ ), water ( $\text{H}_2\text{O}$ ) and carbon monoxide (CO) were measured with a PICARRO G2401 analyzer. Meteorology was measured at all heights with Gill MetPak II Remote weather stations (Gill Instruments Ltd., Hampshire, UK). Data used in this study were taken from the highest height. At Gimmiz (GIM),  $\text{CO}_2$ ,  $\text{CH}_4$ , and  $\text{H}_2\text{O}$  concentrations were measured with a PICARRO G2301, and CO with a Horiba APMA360, which were taken at 32 m a.g.l. The same meteorology instrumentation at Beromünster was employed here. At Früebüel (FRU), which is also a Swiss Fluxnet site (Zeeman et al., 2010),  $\text{CO}_2$ ,  $\text{CH}_4$ , and  $\text{H}_2\text{O}$  concentrations were measured with a PICARRO G2301 at 4 m a.g.l. and meteorology variables were measured at a height of 2 m a.g.l. (Bamberger et al., 2015). On the 32 m tower at Lägern-Hochwacht (LAE),  $\text{CO}_2$ ,  $\text{CH}_4$ , CO, and  $\text{H}_2\text{O}$  concentrations were measured with a PICARRO G2401. Here, MeteoSwiss measured the following meteorological variables: wind (Vaisala WA25 Wind Set, Vaisala Inc., Helsinki, Finland), temperature and humidity (Vaisala HMP155), pressure (Vaisala PTB-220).
- $\text{CO}_2$  and  $\text{CH}_4$  measurements were calibrated against the corresponding international reference scales: WMO X2007 for  $\text{CO}_2$  (Zhao and Tans, 2006), and WMO X2004 for

|  |                              |
|--|------------------------------|
| <a href="#">Title Page</a>               |                              |
| <a href="#">Abstract</a>                 | <a href="#">Introduction</a> |
| <a href="#">Conclusions</a>              | <a href="#">References</a>   |
| <a href="#">Tables</a>                   | <a href="#">Figures</a>      |
| <a href="#">◀</a>                        | <a href="#">▶</a>            |
| <a href="#">◀</a>                        | <a href="#">▶</a>            |
| <a href="#">Back</a>                     | <a href="#">Close</a>        |
| <a href="#">Full Screen / Esc</a>        |                              |
| <a href="#">Printer-friendly Version</a> |                              |
| <a href="#">Interactive Discussion</a>   |                              |



CH<sub>4</sub> (Dlugokencky et al., 2005). The calibration of target gas measurements – not used for the determination of calibration coefficients – suggests an accuracy of the CO<sub>2</sub> and CH<sub>4</sub> measurements of ~ 0.07 ppmv and ~ 0.5 ppbv, respectively, computed as the 10 day averaging window RMSE of individual target measurements during the study period. Except for Früebuel, CO was also continuously measured, and was determined to have an accuracy of ~ 4 ppbv, computed as the 10 day averaging window target RMSE. Measurements were summarized to hourly averages for the one-year period from 1 March 2013 to 28 February 2014 considered in this study.

In order to derive regional signals – the anthropogenic and biospheric contributions within the simulation domain – of the trace gas concentrations at each site, a background concentration was estimated and subtracted from the measurements. The background concentration was estimated using the “robust extraction of baseline signal” method (Ruckstuhl et al., 2012) from measurements at the high Alpine research station Jungfraujoch, which mainly samples free tropospheric air (Zellweger et al., 2003; Henne et al., 2010). Measurements at Jungfraujoch were made with a PICARRO G2401 analyzer and referenced to the same calibration scales (Schibig et al., 2015). We investigated the validity of the assumption that this background concentration estimate corresponds to background concentrations by comparing with the NOAA’s Marine Boundary Layer reference (MBL<sup>1</sup>) at the corresponding latitude. We found them to be very similar (not shown), but the annual peak-to-peak amplitude of the Jungfraujoch background concentration estimate (~ 8 ppmv) is less than that of the MBL estimate (~ 14 ppmv). However, the qualitative purpose of considering regional signals in this study remains unaffected by these differences.

For Switzerland, agricultural CH<sub>4</sub> emissions constitute more than 80 % of the total emissions and show high spatial variation, but their temporal variations are small and predominantly seasonal (Hiller et al., 2014), due to seasonal relocation of cattle. Therefore, within a season, variations of methane concentrations serve as an atmospheric tracer and specifically as a proxy for the effect of the diurnally varying ABL.

<sup>1</sup><http://www.esrl.noaa.gov/gmd/ccgg/mbl/mbl.html>.

|  |                              |
|--|------------------------------|
| <a href="#">Title Page</a>               |                              |
| <a href="#">Abstract</a>                 | <a href="#">Introduction</a> |
| <a href="#">Conclusions</a>              | <a href="#">References</a>   |
| <a href="#">Tables</a>                   | <a href="#">Figures</a>      |
| <a href="#">◀</a>                        | <a href="#">▶</a>            |
| <a href="#">◀</a>                        | <a href="#">▶</a>            |
| <a href="#">Back</a>                     | <a href="#">Close</a>        |
| <a href="#">Full Screen / Esc</a>        |                              |
| <a href="#">Printer-friendly Version</a> |                              |
| <a href="#">Interactive Discussion</a>   |                              |



## 2.2 COSMO meteorology and FLEXPART-COSMO simulations

The sensitivity of the four measurement sites to upwind surface fluxes was assessed using a Lagrangian particle dispersion model (LPDM) driven by meteorological fields from a high resolution numerical weather prediction (NWP) model. As input for the transport simulations we used hourly analysis fields from the operational weather forecast system of the Swiss national weather service MeteoSwiss, which is based on the NWP model COSMO. COSMO is a state-of-the-art non-hydrostatic, limited-area NWP model (Baldauf et al., 2011) developed by the Consortium for Small-Scale Modeling under the guidance of the German weather service DWD (Offenbach, Germany). It is the operational weather forecast model of the national weather services in Germany, Greece, Italy, Poland, Romania, and Russia. In the version COSMO-CLM (Climate Limited area Modeling), optimized for climate simulations, it is used by a wide community of regional climate modelers (<http://www.clm-community.eu>).

The operational setup for COSMO simulations of MeteoSwiss includes two nested domains. The outer domain covers large parts of Europe at about  $7\text{ km} \times 7\text{ km}$  resolution (COSMO-7). The inner domain covers the Alpine region including Switzerland, Austria and parts of Germany, France and Italy at about  $2\text{ km} \times 2\text{ km}$  resolution (COSMO-2). COSMO-7 is driven by European Center for Medium Range Weather Forecast (ECMWF) analysis fields of ECMWF's global IFS model and provides the boundary conditions for the COSMO-2 simulation. Hourly analysis fields are produced for both model domains applying the observational nudging technique (Schraff, 1997) to surface observations of pressure, relative humidity and wind. Similarly, measurements of the same variables plus ambient temperature as taken with sondes and profilers are also assimilated. In addition, a latent heat nudging scheme (Stephan et al., 2008) is used for the COSMO-2 domain to incorporate radar derived rain rates<sup>2</sup>.

COSMO-2 provides the high resolution necessary to represent the complex topography in the alpine area and the topography-induced mesoscale weather patterns. In

<sup>2</sup>For more details see: <http://cosmo-model.org/content/tasks/operational/default.htm>.

Title Page

Abstract

Introduction

Conclusions

References

Tables

Figures

◀

▶

◀

▶

Back

Close

Full Screen / Esc

Printer-friendly Version

Interactive Discussion



order to evaluate the ability of COSMO-2 to represent the local meteorology at the four measurement sites, we interpolated COSMO-2 analysis fields horizontally to each site and vertically to 18 altitude levels between 10 and 3240 m above model ground. This allows us to compare COSMO-2 with meteorological measurements at different heights above ground. Furthermore, it allows assessing the effect of a mismatch between the true altitude of a site and its representation in the model where the topography is smoothed due to the limited model resolution. Although the gentle hill at Beromünster and the flat area around Gimmiz are well represented, the model's elevation at the mountain sites Früebüel and Lägern-Hochwacht are 169 and 274 m, respectively lower than the true elevation. Therefore, we compared COSMO-2 output at two different levels, i.e., at the altitude of the measurement a.s.l. ("true"), and at the measurement height a. m. g. ("model"). The true altitudes and the corresponding model altitudes are summarized in Table 2.

Hourly COSMO analysis fields were used to drive offline atmospheric transport simulations with a modified version of the LPDM FLEXPART (Stohl et al., 2005). FLEXPART simulates the transport and dispersion of infinitesimally small air parcels (referred to as particles) by advective as well as turbulent and convective transport. It can be run either in forward mode (source oriented, i.e. released from sources) or backward mode (receptor oriented, i.e. released backward from receptors). The advective component is calculated from the 3-D wind fields provided by COSMO, and the turbulent transport is based on the scheme of Hanna (1982), which diagnoses ABL and turbulence profiles for stable, neutral and unstable boundary layers based on Monin–Obukhov similarity theory. FLEXPART was modified to run directly on the native grid of COSMO, which is a rotated longitude-latitude grid on a hybrid geometric (i.e. fixed in space) vertical coordinate system. The fact that the original FLEXPART model already operates on a fixed-in-space co-ordinate system greatly facilitated the adaptation to COSMO. In order to be as compatible as possible with the driving NWP model, the same version of the Tiedtke sub-grid convection scheme (Tiedtke, 1989) as used in COSMO-7 was implemented in FLEXPART-COSMO replacing the standard

[Title Page](#)[Abstract](#)[Introduction](#)[Conclusions](#)[References](#)[Tables](#)[Figures](#)[◀](#)[▶](#)[Back](#)[Close](#)[Full Screen / Esc](#)[Printer-friendly Version](#)[Interactive Discussion](#)

Emanuel convection scheme (Forster et al., 2007). Convection is treated as a grid-scale process in COSMO-2 and, hence, no sub-grid convection parameterization is run in either COSMO or FLEXPART-COSMO for the  $2\text{ km} \times 2\text{ km}$  domain. From all four sites, backward transport simulations with FLEXPART-COSMO were started every 3 h to trace the origin of the observed air parcels. In each simulation, 50 000 particles were released from the site's position at site-dependent heights above ground and traced backward in time over 4 days or until they left the simulation domain. The simulations were performed in a nested configuration with COSMO-2 providing the meteorological inputs for the inner domain and COSMO-7 for the outer domain once the particles left the COSMO-2 region. Simulated residence times  $\tau$  ( $\text{s m}^3 \text{ kg}^{-1}$ ; described in Sect. 2.4) were generated for two separate output domains: a high-resolution grid over Switzerland at  $0.02^\circ \times 0.015^\circ$  horizontal resolution extending from  $4.97$  to  $11.05^\circ$  E and  $45.4875$  to  $48.5475^\circ$  N, and a coarser European grid at  $0.16^\circ \times 0.12^\circ$  resolution extending from  $-11.92$  to  $21.04^\circ$  E and  $36.06$  to  $57.42^\circ$  N. Due to the relatively well represented topography at Beromünster and Gimmiz, we chose to release particles at the measurement height above model ground level. The relatively poor representation of topography around Früebüel and Lägern-Hochwacht, however, led us to release particles from a layer between “true” and “model” height rather than from a single height. The particle release heights were chosen based on meteorological evaluation of COSMO presented below and are listed in Table 2.

### 2.3 Land cover dataset

In order to evaluate the sensitivity of the measurement sites to different land cover types (LCT), a dataset of fractional land cover was produced for the FLEXPART-COSMO output domains. The land cover data set consists of LCTs classified according to the land-unit/plant functional type approach used in the land surface model CLM4 (Bonan et al., 2002; Lawrence et al., 2011). Two main sources of land cover data sets were used: the CORINE2006 European land cover data with a resolution of  $100\text{ m} \times 100\text{ m}$  (EEA, 2007) and the MODIS MCD12Q1 IGBP land cover categorization (Friedl et al.,

|  |                              |
|--|------------------------------|
| <a href="#">Title Page</a>               |                              |
| <a href="#">Abstract</a>                 | <a href="#">Introduction</a> |
| <a href="#">Conclusions</a>              | <a href="#">References</a>   |
| <a href="#">Tables</a>                   | <a href="#">Figures</a>      |
| <a href="#">◀</a>                        | <a href="#">▶</a>            |
| <a href="#">◀</a>                        | <a href="#">▶</a>            |
| <a href="#">Back</a>                     | <a href="#">Close</a>        |
| <a href="#">Full Screen / Esc</a>        |                              |
| <a href="#">Printer-friendly Version</a> |                              |
| <a href="#">Interactive Discussion</a>   |                              |



2010) for the reference year 2011 with a resolution of 500 m × 500 m, at locations where CORINE2006 was unavailable. For simplification, we summed plant functional type fractions according to primary plant functional type e.g. temperate evergreen needle-leaf forest plus boreal evergreen needleleaf forest or temperate deciduous broadleaf shrub plus boreal deciduous broadleaf shrub. As expected, the temperate and boreal climate zones comprise all of the simulation domain. Further simplifications of plant functional types were according to leaf phenology of forests; e.g. we summed deciduous broad-leaf and deciduous needle-leaf forest land cover fractions. Furthermore, lakes and wetlands were summed to “Freshwater areas”, and the plant cover type “Bare” and glacier coverage were also summed to “Bare areas”.

## 2.4 Regional surface influence metrics

We define surface sensitivity  $\tau_{100}$  ( $\text{sm}^3 \text{kg}^{-1}$ ) as the residence time of the particles in a 100 m thick layer above model ground divided by the density of dry air in that layer. A layer thickness of 100 m was selected as a compromise between the requirement of selecting a height low enough to be always located in the well-mixed part of the ABL and high enough to allow for a statistically sufficient number of particles in the layer. The results were largely insensitive to this choice as confirmed by comparing with results for  $\tau_{50}$  (50 m) and  $\tau_{200}$  (200 m). Maps of the total residence time summed over the (four-day) simulation period are commonly referred to as footprints and describe the sensitivity of a measurement site to upwind surface fluxes (Seibert and Frank, 2004). For this study only monthly or seasonally averaged residence times were used to characterize the surface influence of the four sites, and are hereafter referred to as mean surface sensitivities,  $\bar{\tau}$ . Further temporally averaged quantities also have an overline.

The spatial sum of monthly mean surface sensitivities, the total surface sensitivity  $\bar{T}_t$ , gives a direct approximation of how much the air parcels arriving at a site have been in contact with the simulation domain's surface during the simulation period, and is

|  |                              |
|--|------------------------------|
| <a href="#">Title Page</a>               |                              |
| <a href="#">Abstract</a>                 | <a href="#">Introduction</a> |
| <a href="#">Conclusions</a>              | <a href="#">References</a>   |
| <a href="#">Tables</a>                   | <a href="#">Figures</a>      |
| <a href="#">◀</a>                        | <a href="#">▶</a>            |
| <a href="#">◀</a>                        | <a href="#">▶</a>            |
| <a href="#">Back</a>                     | <a href="#">Close</a>        |
| <a href="#">Full Screen / Esc</a>        |                              |
| <a href="#">Printer-friendly Version</a> |                              |
| <a href="#">Interactive Discussion</a>   |                              |



defined as

$$\bar{T}_t = \sum_{i,j} \bar{\tau}_{i,j}, \quad (1)$$

where  $i$  and  $j$  are spatial indices.

Short-term variations in observed trace gas concentrations are mainly determined by upwind surface fluxes, which vary with the associated land cover type. In order to investigate influence of different LCTs on each measurement site, monthly LCT contributions  $C_{\text{LCT}}$  were calculated as the weighted mean of LCT fractions  $f_{\text{LCT},i,j}$  over the FLEXPART output grid, using monthly mean surface sensitivities  $\bar{\tau}_{i,j}$  as weights (Eq. 2). With equal surface flux strengths, each LCT would constitute the respective fraction  $C_{\text{LCT}}$  of the observed signal.

$$C_{\text{LCT}} = \frac{1}{\bar{T}_t} \sum_{i,j} \bar{\tau}_{i,j} \cdot f_{\text{LCT},i,j} \quad (2)$$

In order to better gauge the decrease of surface sensitivity with increasing distance, we define the radial surface sensitivity  $\bar{T}_k$  for a site as

$$\bar{T}_k = \frac{1}{\Delta d} \sum_{i,j} \bar{\tau}_{i,j} \quad \forall i,j : \quad d_k < d_{i,j} < d_k + \Delta d, \quad (3)$$

where  $d_{i,j}$  is the great-circle distance of the grid cell with indices  $i$  and  $j$  from the measurement's site position, and the index  $k$  defining a discrete distance bin of width  $\Delta d$ .

In order to compare the area of surface influence of each site, we investigated cumulative surface sensitivities defined as

$$s(\tau) = \sum_{i,j} \bar{\tau}_{i,j} \quad \forall i,j : \quad \bar{\tau}_{i,j} > \tau. \quad (4)$$

|  |                              |
|--|------------------------------|
| <a href="#">Title Page</a>               |                              |
| <a href="#">Abstract</a>                 | <a href="#">Introduction</a> |
| <a href="#">Conclusions</a>              | <a href="#">References</a>   |
| <a href="#">Tables</a>                   | <a href="#">Figures</a>      |
| <a href="#">◀</a>                        | <a href="#">▶</a>            |
| <a href="#">◀</a>                        | <a href="#">▶</a>            |
| <a href="#">Back</a>                     | <a href="#">Close</a>        |
| <a href="#">Full Screen / Esc</a>        |                              |
| <a href="#">Printer-friendly Version</a> |                              |
| <a href="#">Interactive Discussion</a>   |                              |



The area of surface influence is then defined as the region surrounding the site bounded by the isoline  $\tau_{s50}$ , at which the cumulated surface sensitivity includes 50% of the total surface sensitivity:

$$\tau_{s50} : s(\tau_{s50}) = 0.5\bar{T}_t. \quad (5)$$

- 5 Similar metrics were computed by Gloor et al. (2001) using trajectory simulations. They derived a concentration footprint from the decay of the correlation between population density, integrated along the trajectories, and  $C_2Cl_4$  measurements with increasing distance from the measurement site. Although they showed the robustness of their methods, we argue that the independence of  $\bar{T}_k$  and  $\tau_{s50}$  from trace gas measurements and associated surface fluxes constitutes an improvement of the definition of the concentration footprint. Furthermore, the application of an LPDM model that better describes atmospheric transport and dispersion constitutes a clear improvement over their approach but comes at much higher computational cost.
- 10

### 3 Results and discussion

#### 15 3.1 Local site characteristics

The Beromünster site is a 212 m tall, decommissioned radio tower located on a gentle hill in an agricultural area in central Switzerland with an elevation of 797 m.a.s.l. at the base (Fig. 2). Several small farms are located in the vicinity of the tower, and the town of Beromünster (< 7000 inhabitants) is approximately 2 km to the north. The adjacent valley bottoms are at an elevation of approximately 500 and 650 m.a.s.l. Beromünster's surroundings consist of a mosaic of agricultural uses: crops, managed grasslands, and a forested area towards the south.

20 The 32 m tall water tower near Gimmiz is the westernmost site of the network and is located in the flat Seeland region, a former wetland area which was converted to

|  |                              |
|--|------------------------------|
| <a href="#">Title Page</a>               |                              |
| <a href="#">Abstract</a>                 | <a href="#">Introduction</a> |
| <a href="#">Conclusions</a>              | <a href="#">References</a>   |
| <a href="#">Tables</a>                   | <a href="#">Figures</a>      |
| <a href="#">◀</a>                        | <a href="#">▶</a>            |
| <a href="#">◀</a>                        | <a href="#">▶</a>            |
| <a href="#">Back</a>                     | <a href="#">Close</a>        |
| <a href="#">Full Screen / Esc</a>        |                              |
| <a href="#">Printer-friendly Version</a> |                              |
| <a href="#">Interactive Discussion</a>   |                              |



agricultural land in the nineteenth century (Fig. 2). The town of Aarberg (< 5000 inhabitants) is at a distance of approximately 2 km to the southwest, and a farm is situated 200 m to the northeast. The flat area around Gimmiz mainly consists of agricultural plots of seasonal crops, known as the “vegetable garden” of Switzerland. Furthermore, 5 the area directly surrounding Gimmiz is under groundwater protection and further surroundings are under water protection, which means that cattle grazing and use of fertilizer is tightly regulated or forbidden.

About 30 km to the southwest of Beromünster, Früebüel, a Swiss Fluxnet site (Zee- 10 man et al., 2010), is located at an altitude of 987 m a.s.l. on the flank of the gently sloping pre-Alpine Zugerberg, some 500 m above the valley floor (Fig. 3). The region 15 consists of glacial lakes, managed forests and seasonal pastures. The city of Zug 10 km to the north and the small town of Walchwil 2 km to the southwest are the major nearby anthropogenic sources. A small farm is located approximately 300 m to the south. Seasonal pasture surrounds the site, and approximately 50 m to the west there is a small patch of forest, the canopy of which is higher than the measurement inlet at 4 m a.g.l.

The site Lägern-Hochwacht, a 32 m tall tower, is located on the east-west oriented mountain ridge Lägern at an altitude of 840 m a.s.l., and is north of the city of Zurich in the most industrialized and densely settled area of Switzerland (Fig. 3). The terrain falls off steeply to the north and south from the site, and the Lägern crest extends about 20 10 km westwards at similar altitude. Lägern-Hochwacht is surrounded by deciduous and coniferous forest with a maximal canopy height of 20 m.

## Model topography and land cover

Although the main topographic features of Switzerland are represented, the spatial resolution of 2 km creates large differences between true and model topography at the 25 two mountain sites Früebüel and Lägern-Hochwacht (see Table 1 and Fig. 3, second column). In the model topography, the general shape of the Zugerberg remains, but the site's altitude is much lower (169 m). The steep Lägern crest is not identifiable in the model topography, and therefore the site's model altitude is much lower (274 m). On the

[Title Page](#)[Abstract](#)[Introduction](#)[Conclusions](#)[References](#)[Tables](#)[Figures](#)[◀](#)[▶](#)[Back](#)[Close](#)[Full Screen / Esc](#)[Printer-friendly Version](#)[Interactive Discussion](#)

other hand, Beromünster's altitude is slightly lower in the model topography (74 m), but the local topographical features remain identifiable. Furthermore, the plain topography surrounding Gimmiz compares well with the model topography, and the site's model altitude is slightly higher (9 m).

- 5 The land cover in Switzerland is highly fragmented at scales smaller than 2 km (Figs. 2 and 3, third column). The actual variety of land cover, specifically plant functional types, is usually highly simplified in land surface models. Groenendijk et al. (2011) concluded that this simplification may have significant consequences for regional carbon flux modeling, especially in highly heterogeneous landscapes, such as  
10 Switzerland. Therefore, the influence of local fluxes on measured concentrations will still likely be difficult to simulate even at this relatively high resolution.

### 3.2 Local meteorology and diurnal cycle

The measured wind roses indicate frequent air flow channeling between the Jura mountain range and the Alps, resulting in either southwesterly or northeasterly wind directions (Fig. 4). Früebühl is an exception, where the local environment likely redirects prevailing winds. Due to the highest measurement altitude, Beromünster observed the highest windspeeds. At Gimmiz, lower windspeeds due to lower measurement altitude and high frequency of northeasterly winds, colloquially known as "Bise", are measured. Früebühl occasionally observes strong winds from southeasterly directions during Foehn events (Bamberger et al., 2015). Similar to Beromünster, Lägern-Hochwacht observed high windspeeds, which were highly channeled from either northeast or southwest.

At Beromünster, the diurnal cycles of measured windspeed show higher values during nighttime than daytime indicating presence in the mixed layer during daytime and transition to the nocturnal residual layer during nighttime (Figs. 5 and 6). In summer, specific humidity exhibits an increase between 07:00 and 10:00 UTC (08:00–11:00 LT) and a simultaneous decrease in windspeed, which likely occurs as the expanding mixed layer gradually ascends past the tower top. The peak of specific humidity cor-

[Title Page](#)[Abstract](#)[Introduction](#)[Conclusions](#)[References](#)[Tables](#)[Figures](#)[◀](#)[▶](#)[◀](#)[▶](#)[Back](#)[Close](#)[Full Screen / Esc](#)[Printer-friendly Version](#)[Interactive Discussion](#)

responds temporally to that of summertime regional methane signals ( $\Delta\text{CH}_4$ ), further indicating mixed layer influence. Summertime regional  $\text{CO}_2$  signals ( $\Delta\text{CO}_2$ ) show only a small diurnal ( $\pm 4$  ppmv) variability, which corresponds to the expectation of a weak signal from diurnal surface flux variations at the top of a tall tower (Andrews et al., 2014). Wintertime diurnal variability is hardly discernible in both  $\text{CO}_2$  and  $\text{CH}_4$  concentrations, indicating a weak influence of ABL dynamics.

At Gimmiz, the increase in windspeed during the day and decrease during the night indicates constant presence of the measurement inlet in the surface layer, contrary to Beromünster (Figs. 5 and 6). In summer and winter,  $\text{CO}_2$  and  $\text{CH}_4$  are negatively correlated with windspeed, further emphasizing the influence of diurnal ABL dynamics. The nighttime increase of more than 60 ppmv suggests rapid accumulation of respiration  $\Delta\text{CO}_2$  in the shallow nocturnal boundary layer. Nocturnal regional advection of  $\Delta\text{CO}_2$  may also contribute to the nighttime enrichment (Eugster and Siegrist, 2000), although low windspeeds at night suggest that the surface influence is limited to a few tens of kilometers from the site. Both the high wintertime  $\text{CO}_2$  concentrations (30 ppmv above background), and the high correlation between wintertime  $\Delta\text{CH}_4$  and  $\Delta\text{CO}_2$  indicate that wintertime diurnal ABL dynamics are responsible for observed diurnal variability. Please note that the winter was atypically mild ( $2.3^\circ\text{C}$  above the norm from 1961–1990; MeteoSwiss, 2014) for regions north of the Alpine divide, which would have caused increased wintertime respiration, and contributed to the high observed  $\text{CO}_2$  concentrations.

At Früebüel, the large magnitude in the temperature daily cycle, the low measured windspeeds, and the high humidity indicate strong surface influence (Figs. 7 and 8), and is consistent with the near-surface measurement height. During summer,  $\text{CO}_2$  concentrations decreased in the morning along with an increase in temperature and humidity, both before windspeed increased. This typifies influence of photosynthetic activity, and further indicates strong local surface influence.

The second mountaintop site Lägern-Hochwacht shows a similar behavior to Beromünster with a delayed increase in daytime temperatures and higher windspeeds

[Title Page](#)[Abstract](#)[Introduction](#)[Conclusions](#)[References](#)[Tables](#)[Figures](#)[◀](#)[▶](#)[◀](#)[▶](#)[Back](#)[Close](#)[Full Screen / Esc](#)[Printer-friendly Version](#)[Interactive Discussion](#)

at night than during the day (Figs. 7 and 8). Especially during summer, the diurnal cycles of measured windspeed show higher values during nighttime than daytime, which indicates a shift from the mixed layer during daytime to the residual layer during nighttime, and an increased influence of nocturnal jets. Specific humidity exhibits an increase between 06:00 and 09:00 UTC (07:00–10:00 LT) and a simultaneous decrease in windspeed, further indicating a shift to the mixed layer. The delay in the decrease of  $\Delta\text{CO}_2$  and peak of  $\Delta\text{CH}_4$  at 09:00 UTC indicate upward mixing of air containing nocturnally accumulated  $\text{CO}_2$  and  $\text{CH}_4$ , which we also observe at Beromünster. On average, the mixed layer begins to influence Lägern-Hochwacht measurements an hour earlier than at Beromünster. During winter, the additional 5 ppmv offset compared to Früebüel in the flat diurnal cycle of  $\Delta\text{CO}_2$  and  $\Delta\text{CH}_4$  concentrations indicates nearby anthropogenic sources, and weak influence from ABL dynamics, respectively.

## COSMO-2 meteorology evaluation

Beromünster's simulated wind roses compare well with the observed wind roses, but high windspeeds are simulated too frequently (Fig. 4). Simulated and measured diurnal cycles agree well in all seasons, and simulations at the measurement height above model ground level at 212 m agree slightly better (Figs. 5 and 6). Small differences from the measurements include an overestimation of windspeeds in the afternoon in summer, and a delayed and too small increase in temperature during winter.

At Früebüel, neither the dominating wind directions nor the wind speeds are well reproduced by the COSMO-2 model suggesting strong localized influences on wind patterns. The lowest model output level (10 m a.g.l.) compares best with the near-surface meteorological characteristics of Früebüel. Because the model is evaluated at the center of the lowest model layer at about 10 m a.g.l. and the meteorological measurements are closer to the surface at 2 m a.g.l., a general overestimation of windspeeds is expected. The timing of simulated and measured diurnal variations of humidity and windspeed correspond, but humidity is biased low and windspeed is biased high throughout the day. Furthermore, the amplitude of the daily temperature cycle is underestimated,

## Greenhouse gas observation network characterization

B. Oney et al.

[Title Page](#)

[Abstract](#)

[Introduction](#)

[Conclusions](#)

[References](#)

[Tables](#)

[Figures](#)

◀

▶

◀

▶

[Back](#)

[Close](#)

[Full Screen / Esc](#)

[Printer-friendly Version](#)

[Interactive Discussion](#)



most notably in winter. On the other hand, simulated wintertime temperatures show a warm bias even at the true station height, well above the surface.

At Gimmiz, the simulated wind roses compare well, but a small bias in the north-eastern wind direction exists. The diurnal cycle simulations agree well with the measurements in summer and winter. However, simulated nighttime temperature and wind-speed are overestimated suggesting a too well mixed nighttime ABL, which in an inverse modeling framework would likely lead to an overestimation of nighttime respiration, due to an overly diluted trace gas signal.

In the highly smoothed model topography, Lägern-Hochwacht is more similar to Beromünster (compare cyan lines in Figs. 2b and 3b). Therefore, the rotation to a more north-southerly axis of observed winds is most likely a local topographic effect exerted by the east-west oriented ridge on the prevailing southwesterly and northeasterly winds. The wintertime simulated temperature is too high on average at all heights shown, similar to Früebüel. The measured meteorology is usually bracketed by the simulations evaluated at 32 m a.m.g. and at the true height (306 m a.m.g.), indicating that the site would be represented best by an intermediate simulation height.

Where the “model” and “true” topography are similar, simulated and measured meteorology show good agreement for Beromünster and Gimmiz. Contrastingly, local meteorology is not reproduced accurately at the mountaintop sites due likely to the smoothed model topography. The relatively poor meteorology simulations could cause problems with simulating trace gas observations if either the influence of local sources and sinks near the site were important and not well represented, or the local topography or meteorology induces vertical transport that the transport model misrepresents.

At Beromünster and Gimmiz, where “true” and “model” topography differs little, measurement and simulations agree best at the measurement height above model ground level. For Früebüel and Lägern-Hochwacht, the optimal simulation height above model ground, according to the meteorology evaluation, appears to be between the “model” measurement height and the “true” measurement height.

[Title Page](#)[Abstract](#)[Introduction](#)[Conclusions](#)[References](#)[Tables](#)[Figures](#)[◀](#)[▶](#)[◀](#)[▶](#)[Back](#)[Close](#)[Full Screen / Esc](#)[Printer-friendly Version](#)[Interactive Discussion](#)

**Greenhouse gas observation network characterization**

B. Oney et al.

[Title Page](#)[Abstract](#)[Introduction](#)[Conclusions](#)[References](#)[Tables](#)[Figures](#)[|◀](#)[▶|](#)[◀](#)[▶](#)[Back](#)[Close](#)[Full Screen / Esc](#)[Printer-friendly Version](#)[Interactive Discussion](#)

### 3.3 Regional surface influence

#### 3.3.1 Measured regional signals

Over the Swiss Plateau, daytime monthly averaged regional CO<sub>2</sub> signals ( $\Delta\text{CO}_2$ ) vary from -5 ppmv during warm summer days to +15 ppmv during cold winter days (Fig. 9a and b). During the warmer months at daytime, intense vertical mixing caused regional CO<sub>2</sub> signals to be similar across sites. During the months of May and November, stormy weather reduced diurnal variation and the differences in regional signals between sites.

With a similar temporal pattern to CO<sub>2</sub> regional signals, daytime monthly averaged regional CH<sub>4</sub> signals ( $\Delta\text{CH}_4$ ) vary from +0.05 ppmv (+50 ppbv) during warm summer days to +0.1 ppmv (+100 ppbv) during cold winter days (Fig. 9c and d). Due to the same meteorological conditions conducive to vertical mixing during summer days and the months of May and November, regional CH<sub>4</sub> signals are similar across the measurement network.

On the other hand, the atmospheric stratification that accompanies reduced solar heating caused regional signals to differ more between measurement sites during nighttime and winter. For example, the cold and fair weather during December and associated high atmospheric stratification reduced diurnal variation and increased the differences between sites. Furthermore, due to a combination of site characteristics and atmospheric stratification, regional signals differed most between Beromünster and Gimmiz.

The small diurnal variation of observed regional CO<sub>2</sub> and CH<sub>4</sub> signals at Beromünster is expected, being vertically distant enough from the surrounding land surface to rarely observe nocturnal respiration fluxes. This damped signal contrasts that of the other sites and is often similar to the daytime measurement values of other sites. Interestingly, summer nighttime measurements are similar to the background estimate. Also, the higher daytime regional CH<sub>4</sub> signals during summertime coincide with the location in an area of very high cattle density (Hiller et al., 2014). During winter, relatively low CO<sub>2</sub> measurements indicate minimal anthropogenic influence.

The large diurnal variation in both of the observed regional signals at Gimmiz is difficult to understand. The strong CO<sub>2</sub> signals are likely related to the combination of fluxes from nearby settlements and crops and a stable nocturnal boundary layer. The summertime peak in nighttime regional signals points toward a biogenic cause.

Both the high water table and the practice of till farming may also contribute to the biogenic CO<sub>2</sub> fluxes, and the high water table would aid understanding of the strong CH<sub>4</sub> signals. Again, the strong nighttime regional signals may also be due to nocturnal regional advection of CO<sub>2</sub> (Eugster and Siegrist, 2000), although low windspeeds do not support this hypothesis.

At Früebühl, local topography is not conducive to a stable nocturnal surface layer, and therefore the nighttime regional CO<sub>2</sub> signals are likely not as high as would be expected in flat terrain. The summertime peak in nighttime regional CO<sub>2</sub> signals is not as intense as Gimmiz, but shows similar annual variation, pointing towards respiration fluxes. As at Beromünster, relatively low wintertime CO<sub>2</sub> measurements indicate minimal anthropogenic influence.

The higher daytime regional CH<sub>4</sub> signals during summertime coincide with the location in an area of high cattle density, also similar to Beromünster. Interestingly, regional CH<sub>4</sub> signals do not seem influenced by the cattle grazing on the pastures directly surrounding Früebühl during the months of June and December (Bamberger et al., 2015).

At Lägern-Hochwacht, observed diurnal variation of regional CO<sub>2</sub> signals is small, similar to Beromünster (Fig. 9). During winter, the elevated day- and nighttime regional signals indicate a strong anthropogenic influence, which aligns with the surrounding industrialized area. Furthermore, the daytime values of both ΔCO<sub>2</sub> and ΔCH<sub>4</sub> are higher than at nighttime, which indicates either similar sources or, more likely, a polluted tem-

perature inversion layer thermally expanding during the day and contracting during the night.

[Title Page](#)[Abstract](#)[Introduction](#)[Conclusions](#)[References](#)[Tables](#)[Figures](#)[|◀](#)[▶|](#)[◀](#)[▶](#)[Back](#)[Close](#)[Full Screen / Esc](#)[Printer-friendly Version](#)[Interactive Discussion](#)

### 3.3.2 Simulated surface influence

The monthly total surface sensitivities ( $\bar{T}_t$ ) differ most between sites during periods of higher atmospheric stratification (Fig. 9e and f), which is mainly due to the difference between particle release altitude at the site and average altitude of the surrounding (< 500 km) land surfaces. Therefore, the difference between Beromünster and Gimmiz is greatest, and results from being located on a tall tower on top of a hill or on a flat plain on a small tower with associated particle release altitudes at 1014 and 485 m.a.s.l., respectively. In short, air parcels arriving at Gimmiz had the most contact with the land surface, whereas air parcels arriving at Beromünster had the least contact with the land surface.

The annual variation of the total surface sensitivities is very similar to the observed regional greenhouse gas signals, which indicates qualitative success in simulating surface sensitivity (Fig. 9). For example, during the warmer months at daytime, increased vertical mixing causes total surface sensitivities to be similar across sites.

During the months of May and November, stormy weather also reduced differences between sites. Total surface sensitivity differences between measurement sites increased during nighttime and winter, similar to the regional signals. Again, the cold and clear weather during December and associated high air mass stratification reduced diurnal variation and caused increased the differences between sites. That is, for the same reasons we qualitatively understand annual and diurnal variation in regional signals, we can understand variation in total surface sensitivity.

Monthly land cover type (LCT) contributions  $C_{LCT}$  vary little throughout the year, and on average reflect the typical land cover for Switzerland and Central Europe (Fig. 10). At all sites, forest similarly influences the arriving air parcels by about ~30 %, and a variable combination of crops and grasslands constitutes most of the surface influence (combined ~50–60 %). For example in Fig. 10a, air parcels, which were observed during the month of March 2013 at Beromünster and were in contact with the surface, spent approximately 20 % of the time over the evergreen forest LCT, 10 % of the time

|  |                              |
|--|------------------------------|
| <a href="#">Title Page</a>               |                              |
| <a href="#">Abstract</a>                 | <a href="#">Introduction</a> |
| <a href="#">Conclusions</a>              | <a href="#">References</a>   |
| <a href="#">Tables</a>                   | <a href="#">Figures</a>      |
| <a href="#">◀</a>                        | <a href="#">▶</a>            |
| <a href="#">◀</a>                        | <a href="#">▶</a>            |
| <a href="#">Back</a>                     | <a href="#">Close</a>        |
| <a href="#">Full Screen / Esc</a>        |                              |
| <a href="#">Printer-friendly Version</a> |                              |
| <a href="#">Interactive Discussion</a>   |                              |



over the deciduous forest LCT, 20 % over the grassland LCT, and 30 % over the crop LCT.

Given the contrasting meteorological conditions of night and day, and winter and summer, mean surface sensitivity generally decreased with increasing distance from the sites (Fig. 11), as expected. The average distance at which 50 % of the total sensitivity had accumulated is between 50 km (summer nighttime and winter) and 300 km (summer daytime) and is larger for Beromünster and Lägern-Hochwacht than for Früebühl and Gimmiz (Fig. 11, vertical dotted lines).

The areas of surface influence exhibit much geographic overlap during periods of increased vertical mixing, during summer days, and are smaller and overlap less during periods of decreased vertical mixing, at night and during winter (Fig. 12). In the summer afternoon, all sites exhibit a similar area of surface influence due to the rapid vertical mixing in the mixed layer. The northeast-southwest orientation of the areas of surface influence is consistent with observed air flow channeling between the Jura mountain range and the Alps (Fig. 4). Abnormally frequent southerly winds during January and February 2014 caused areas of surface influence to be pronounced towards the south during the winter.

When considering the area of surface influence or the distance-dependent decay of surface sensitivity during periods of higher atmospheric stratification, Gimmiz and Früebühl are similar and Beromünster and Lägern-Hochwacht are also similar. This shows the effect of presence within the surface layer on surface sensitivity. That is, presence within the surface layer usually results in a sharp decrease of surface sensitivity with distance, and a correspondingly small area of surface influence as seen at Gimmiz and Früebühl. Contrastingly, the location above the surface layer during periods of higher atmospheric stratification results in an initial increase of surface sensitivity with distance before decreasing, and results in a relatively large area of surface influence as seen at Beromünster and Lägern-Hochwacht at nighttime and during winter.

Beromünster exhibits the lowest total surface sensitivity of the sites (Fig. 9), and surface sensitivity initially increases before decreasing (except summer afternoon) as

[Title Page](#)[Abstract](#)[Introduction](#)[Conclusions](#)[References](#)[Tables](#)[Figures](#)[|◀](#)[▶|](#)[◀](#)[▶](#)[Back](#)[Close](#)[Full Screen / Esc](#)[Printer-friendly Version](#)[Interactive Discussion](#)

distance from the measurement site position increases (Fig. 11). Here, we find the conceptual understanding of the exponential decay of surface sensitivity with increasing distance from a tall tower site, as presented by Gloor et al. (2001), to be valid only during well mixed conditions (Fig. 11c). The area of surface influence is the largest of all sites on average (Fig. 12), as expected. Beromünster exhibits high sensitivity to grasslands, which, along with being located in an intense dairy farming area (Hiller et al., 2014), would likely increase sensitivity to agricultural methane emissions. The LCTs observed at Beromünster represent typical land cover for Switzerland.

Gimmiz exhibits a high total surface influence (Fig. 9) that decreases sharply with increasing distance from the site (Fig. 11). The area of surface influence for Gimmiz covers the Seeland on average (Fig. 12). Opposite to Beromünster, the cold and clear weather during December caused increased coupling to the nearby surface (< 50 km, Fig. 11) and higher total surface sensitivity (Fig. 9), which corresponds to the small wintertime area of surface influence (Fig. 12). Gimmiz exhibits a high sensitivity to crop LCTs (Fig. 10), which is due to pronounced near-field surface sensitivity (especially in December) and the intense agricultural activity typical of the Seeland region. Qualitative understanding of the observed higher wintertime CO<sub>2</sub> at Gimmiz (Fig. 9) is aided by the higher surface sensitivity to urban areas (Fig. 10).

Früebüel exhibits an area of surface influence pronounced to the south, covering the immediate prealpine area well (Fig. 12). Due to the frequent presence in the surface layer, the surface sensitivity decreases quickly with increasing distance (Fig. 11). Total surface sensitivity at Früebüel during wintertime is relatively small (Fig. 9). This is likely due to the higher particle release altitude (853–913 m a.s.l.) and corresponding vertical distance from the average altitude of the Swiss Plateau (~ 450 m a.s.l.). Similar to Beromünster, Früebüel exhibits high sensitivity to grasslands (Fig. 10), and thereby increased sensitivity to methane emissions (Hiller et al., 2014). Früebüel shows the highest sensitivity to “Bare”, alpine areas and “Freshwater areas”, due to the proximity to the Alps, and the many nearby prealpine lakes.

[Title Page](#)[Abstract](#)[Introduction](#)[Conclusions](#)[References](#)[Tables](#)[Figures](#)[◀](#)[▶](#)[Back](#)[Close](#)[Full Screen / Esc](#)[Printer-friendly Version](#)[Interactive Discussion](#)

|  |                              |
|--|------------------------------|
| <a href="#">Title Page</a>               |                              |
| <a href="#">Abstract</a>                 | <a href="#">Introduction</a> |
| <a href="#">Conclusions</a>              | <a href="#">References</a>   |
| <a href="#">Tables</a>                   | <a href="#">Figures</a>      |
| <a href="#">◀</a>                        | <a href="#">▶</a>            |
| <a href="#">◀</a>                        | <a href="#">▶</a>            |
| <a href="#">Back</a>                     | <a href="#">Close</a>        |
| <a href="#">Full Screen / Esc</a>        |                              |
| <a href="#">Printer-friendly Version</a> |                              |
| <a href="#">Interactive Discussion</a>   |                              |



The surface sensitivity as a function of distance (Fig. 11) and area of surface influence (Fig. 12) of Lägern-Hochwacht show similarity to those of Beromünster. Total surface sensitivities are greater than those of Beromünster, but less than those of the other sites (Fig. 9), which the relatively large areas of surface influence also indicate.

- 5 The comparably high sensitivity to distant surfaces is due to the elevated release height and small vertical distance from surrounding land surfaces. The particle release altitudes are lower (666–766 m a.s.l.) than Beromünster or Früebühl and thereby vertically closer to the average Swiss Plateau altitude (~ 450 m a.s.l.). This results in relatively higher total surface sensitivity during periods of increased atmospheric stratification
- 10 (Fig. 9), which, with the increased sensitivity to urban areas (Fig. 10), help to qualitatively explain comparably high observed wintertime CO<sub>2</sub> concentrations.

## 4 Conclusions

The four measurement sites of the CarboCount CH network provide complementary data sets to constrain emissions from the Swiss Plateau, but would not be useful for constraining emissions south of the Alpine divide, for example. At Gimmiz and Früebühl, the local environment exerts much influence, causing strong local signals to dominate the time-series. Therefore, a measurement data filter to remove the strong local signal will be necessary for the Früebühl measurements and likely for the Gimmiz measurements. On the other hand, the local environment (< 10 km) exerts little influence

15 on the measurements made at Beromünster and Lägern-Hochwacht, where mainly regional-scale signals are observed.

Measurement sites in complex terrain still present formidable challenges for numerical weather prediction and thereby atmospheric transport modeling. The differences we found between simulated and measured local meteorology are likely due to differences between true and model topography. The ability to simulate local meteorology likely translates into the ability to accurately simulate local surface influence, which is

20 an important aspect to simulate due to the potentially large contribution of local sur-

face fluxes to observed greenhouse gas concentration variation, such as at the sites Früebüel and Gimmiz. Furthermore, the requirements for the spatial density and infrastructure of the measurement network are driven by periods of high atmospheric stratification and by local wind patterns. For example, due to the likely constant presence in the surface layer and resulting highly variable area of surface influence, the time-series from Gimmiz is mainly useful for constraining Swiss Plateau emissions during warm days, although the tower is the same height as the tower at Lägern-Hochwacht. We recommend similar meteorological model evaluation and regional influence studies when making preliminary considerations about measurement network design and deployment.

Land cover and vegetation types influencing arriving air parcel concentrations vary little throughout the year and differences between sites are due to proximal (< 50 km) land cover. Nonetheless, the observed greenhouse gas concentrations differ substantially between sites. Thus, the collected information-rich datasets present a formidable challenge for terrestrial carbon flux modelers.

**Acknowledgements.** This study was funded by the Swiss National Funds (SNF) as part of the “CarboCount CH” Sinergia Project (Grant Number: CRSII2\_136273). We acknowledge the use of the Jungfraujoch trace gas measurements carried out by Martin Steinbacher, Empa, in the framework of the Integrated Carbon Observation System in Switzerland (ICOS-CH), SNF Grant 20FI21\_1489921. We also acknowledge MeteoSwiss for the provision of their operational COSMO analysis products and of the meteorological measurements at Lägern-Hochwacht. Swiss Fluxnet is acknowledged for the meteorological measurements at Früebüel. We thank Tesfaye Berhanu and Lukas Emmenegger for reading draft versions and giving helpful comments.

|                                   |  |                              |
|-----------------------------------|--|------------------------------|
| <a href="#">Title Page</a>        | <a href="#">Abstract</a>                 | <a href="#">Introduction</a> |
| <a href="#">Conclusions</a>       | <a href="#">References</a>               |                              |
| <a href="#">Tables</a>            | <a href="#">Figures</a>                  |                              |
| <a href="#">◀</a>                 | <a href="#">▶</a>                        |                              |
| <a href="#">◀</a>                 | <a href="#">▶</a>                        |                              |
| <a href="#">Back</a>              | <a href="#">Close</a>                    |                              |
| <a href="#">Full Screen / Esc</a> |  |                              |
|                                   | <a href="#">Printer-friendly Version</a> |                              |
|                                   | <a href="#">Interactive Discussion</a>   |                              |



## References

- Andreae, M. O., Artaxo, P., Brandão, C., Carswell, F. E., Ciccioli, P., da Costa, A. L., Culf, A. D., Esteves, J. L., Gash, J. H. C., Grace, J., Kabat, P., Lelieveld, J., Malhi, Y., Manzi, A. O., Meixner, F. X., Nobre, A. D., Nobre, C., Ruivo, M. d. L. P., Silva-Dias, M. A., Stefani, P., Valentini, R., von Jouanne, J., and Waterloo, M. J.: Biogeochemical cycling of carbon, water, energy, trace gases, and aerosols in Amazonia: the LBA-EUSTACH experiments, *J. Geophys. Res.*, 107, 1–25, doi:10.1029/2001JD000524, 2002. 12914
- Andrews, A. E., Kofler, J. D., Trudeau, M. E., Williams, J. C., Neff, D. H., Masarie, K. A., Chao, D. Y., Kitzis, D. R., Novelli, P. C., Zhao, C. L., Dlugokencky, E. J., Lang, P. M., Crotwell, M. J., Fischer, M. L., Parker, M. J., Lee, J. T., Baumann, D. D., Desai, A. R., Stanier, C. O., De Wekker, S. F. J., Wolfe, D. E., Munger, J. W., and Tans, P. P.: CO<sub>2</sub>, CO, and CH<sub>4</sub> measurements from tall towers in the NOAA Earth System Research Laboratory's Global Greenhouse Gas Reference Network: instrumentation, uncertainty analysis, and recommendations for future high-accuracy greenhouse gas monitoring efforts, *Atmos. Meas. Tech.*, 7, 647–687, doi:10.5194/amt-7-647-2014, 2014. 12926
- Bakwin, P., Tans, P., Hurst, D., and Zhao, C.: Measurements of carbon dioxide on very tall towers: results of the NOAA/CMDL program, *Tellus B*, 50, 401–415, doi:10.1034/j.1600-0889.1998.t01-4-00001.x, 1998. 12914
- Baldau, M., Seifert, A., Förstner, J., Majewski, D., Raschendorfer, M., and Reinhardt, T.: Operational convective-scale numerical weather prediction with the COSMO model: description and sensitivities, *Mon. Weather Rev.*, 139, 3887–3905, doi:10.1175/MWR-D-10-05013.1, 2011. 12918
- Baldocchi, D., Falge, E., Gu, L., Olson, R., Hollinger, D., Running, S., Anthoni, P., Bernhofer, C., Davis, K., Evans, R., Fuentes, J., Goldstein, A., Katul, G., Law, B., Lee, X., Malhi, Y., Meyers, T., Munger, W., Oechel, W., Paw U, K. T., Pilegaard, K., Schmid, H. P., Valentini, R., Verma, S., Vesala, T., Wilson, K., and Wofsy, S.: FLUXNET: a new tool to study the temporal and spatial variability of ecosystem-scale carbon dioxide, water vapor, and energy flux densities, *B. Am. Meteorol. Soc.*, 82, 2415–2434, doi:10.1175/1520-0477(2001)082<2415:FANTTS>2.3.CO;2, 2001. 12914

## Greenhouse gas observation network characterization

B. Oney et al.

[Title Page](#)

[Abstract](#)

[Introduction](#)

[Conclusions](#)

[References](#)

[Tables](#)

[Figures](#)

◀

▶

[Back](#)

[Close](#)

[Full Screen / Esc](#)

[Printer-friendly Version](#)

[Interactive Discussion](#)



Bamberger, I., Oney, B., Brunner, D., Henne, S., Leuenberger, M., Buchmann, N., and Eugster, W.: Observation of atmospheric methane and carbon dioxide mixing ratios: Tall tower or mountain top stations?, in preparation, 2015. 12916, 12925, 12930

5 Battle, M., Bender, M., Tans, P. P., White, J., Ellis, J., Conway, T., and Francey, R.: Global carbon sinks and their variability inferred from atmospheric O<sub>2</sub> and δ<sup>13</sup>C, *Science*, 287, 2467–2470, 2000. 12913

Bonan, G. B., Levis, S., Kergoat, L., and Oleson, K. W.: Landscapes as patches of plant functional types: an integrating concept for climate and ecosystem models, *Global Biogeochem. Cy.*, 16, 1–23, doi:10.1029/2000GB001360, 2002. 12920

10 Ciais, P., Dolman, A. J., Bombelli, A., Duren, R., Peregón, A., Rayner, P. J., Miller, C., Gobron, N., Kinderman, G., Marland, G., Gruber, N., Chevallier, F., Andres, R. J., Balsamo, G., Bopp, L., Bréon, F.-M., Broquet, G., Dargaville, R., Battin, T. J., Borges, A., Bovensmann, H., Buchwitz, M., Butler, J., Canadell, J. G., Cook, R. B., DeFries, R., Engelen, R., Gurney, K. R., Heinze, C., Heimann, M., Held, A., Henry, M., Law, B., Luysaert, S., Miller, J., Moriyama, T., Moulin, C., Myneni, R. B., Nussli, C., Obersteiner, M., Ojima, D., Pan, Y., Paris, J.-D., Piao, S. L., Poulter, B., Plummer, S., Quegan, S., Raymond, P., Reichstein, M., Rivier, L., Sabine, C., Schimel, D., Tarasova, O., Valentini, R., Wang, R., van der Werf, G., Wickland, D., Williams, M., and Zehner, C.: Current systematic carbon-cycle observations and the need for implementing a policy-relevant carbon observing system, *Biogeosciences*, 11, 3547–3602, doi:10.5194/bg-11-3547-2014, 2014. 12913, 12914

Crosson, E. R.: A cavity ring-down analyzer for measuring atmospheric levels of methane, carbon dioxide, and water vapor, *Appl. Phys. B*, 92, 403–408, doi:10.1007/s00340-008-3135-y, 2008. 12916

25 Dlugokencky, E. J., Myers, R. C., Lang, P. M., Masarie, K. A., Crotwell, A. M., Thoning, K. W., Hall, B. D., Elkins, J. W., and Steele, L. P.: Conversion of NOAA atmospheric dry air CH<sub>4</sub> mole fractions to a gravimetrically prepared standard scale, *J. Geophys. Res.*, 110, D18306, doi:10.1029/2005JD006035, 2005. 12917

30 Dolman, A. J., Tolk, L., Ronda, R., Noilhan, J., Sarrat, C., Brut, A., Piguet, B., Durand, P., Butet, A., Jarosz, N., Brunet, Y., Loustau, D., Lamaud, E., Miglietta, F., Gioli, B., Magliulo, V., Esposito, M., Gerbig, C., Körner, S., Glademard, P., Ramonet, M., Ciais, P., Neininger, B., Hutjes, R. W. A., Elbers, J. A., Macatangay, R., Schrems, O., Pérez-Landa, G., Sanz, M. J., Scholz, Y., Facon, G., Ceschia, E., and Beziat, P.: The CarboEurope Regional Experi-

|  |                              |
|--|------------------------------|
| <a href="#">Title Page</a>               |                              |
| <a href="#">Abstract</a>                 | <a href="#">Introduction</a> |
| <a href="#">Conclusions</a>              | <a href="#">References</a>   |
| <a href="#">Tables</a>                   | <a href="#">Figures</a>      |
| <a href="#">◀</a>                        | <a href="#">▶</a>            |
| <a href="#">◀</a>                        | <a href="#">▶</a>            |
| <a href="#">Back</a>                     | <a href="#">Close</a>        |
| <a href="#">Full Screen / Esc</a>        |                              |
| <a href="#">Printer-friendly Version</a> |                              |
| <a href="#">Interactive Discussion</a>   |                              |



ment Strategy, *B. Am. Meteorol. Soc.*, 87, 1367–1379, doi:10.1175/BAMS-87-10-1367, 2006.  
12914

5 Dolman, A. J., Gerbig, C., Noilhan, J., Sarrat, C., and Miglietta, F.: Detecting regional variability in sources and sinks of carbon dioxide: a synthesis, *Biogeosciences*, 6, 1015–1026, doi:10.5194/bg-6-1015-2009, 2009. 12914

EEA: CLC 2006 Technical Guidelines, European Environment Agency, Technical Report No. 17/2007, 1–70, Office for Official Publications of the European Communities, Copenhagen, Denmark, available at: [http://www.eea.europa.eu/publications/technical\\_report\\_2007\\_17](http://www.eea.europa.eu/publications/technical_report_2007_17) (last access: 6 June 2014), 2007. 12920

10 Eugster, W. and Siegrist, F.: The influence of nocturnal CO<sub>2</sub> advection on CO<sub>2</sub> flux measurements, *Basic Appl. Ecol.*, 1, 177–188, 2000. 12926, 12930

Forster, C., Stohl, A., and Seibert, P.: Parameterization of convective transport in a Lagrangian particle dispersion model and its evaluation, *J. Appl. Meteorol. Clim.*, 46, 403–422, doi:10.1175/JAM2470.1, 2007. 12920

15 Friedl, M. A., Sulla-Menashe, D., Tan, B., Schneider, A., Ramankutty, N., Sibley, A., and Huang, X.: MODIS Collection 5 global land cover: algorithm refinements and characterization of new datasets, *Remote Sens. Environ.*, 114, 168–182, doi:10.1016/j.rse.2009.08.016, 2010. 12920

20 Gerbig, C., Lin, J. C., Wofsy, S. C., Daube, B. C., Andrews, A. E., Stephens, B. B., Bakwin, P. S., and Grainger, C. A.: Toward constraining regional-scale fluxes of CO<sub>2</sub> with atmospheric observations over a continent: 2. Analysis of COBRA data using a receptor-oriented framework, *J. Geophys. Res.-Atmos.*, 108, 1–14, 2003a. 12914

25 Gerbig, C., Lin, J. C., Wofsy, S. C., Daube, B. C., Andrews, A. E., Stephens, B. B., Bakwin, P. S., and Grainger, C. A.: Toward constraining regional-scale fluxes of CO<sub>2</sub> with atmospheric observations over a continent: 1. Observed spatial variability from airborne platforms, *J. Geophys. Res.-Atmos.*, 108, 1–27, 2003b. 12914

30 Gerbig, C., Dolman, A. J., and Heimann, M.: On observational and modelling strategies targeted at regional carbon exchange over continents, *Biogeosciences*, 6, 1949–1959, doi:10.5194/bg-6-1949-2009, 2009. 12913, 12915

Gloor, M., Bakwin, P., Hurst, D., Lock, L., Draxler, R., and Tans, P.: What is the concentration footprint of a tall tower?, *J. Geophys. Res.*, 106, 17831–17840, doi:10.1029/2001JD900021, 2001. 12923, 12933

Title Page

Abstract

Introduction

Conclusions

References

Tables

Figures

◀

▶

◀

▶

Back

Close

Full Screen / Esc

Printer-friendly Version

Interactive Discussion



- Groenendijk, M., Dolman, A., Van Der Molen, M., Leuning, R., Arneth, A., Delpierre, N., Gash, J., Lindroth, A., Richardson, A., Verbeeck, H., and Wohlfahrt, G.: Assessing parameter variability in a photosynthesis model within and between plant functional types using global Fluxnet eddy covariance data, *Agr. Forest Meteorol.*, 151, 22–38, doi:10.1016/j.agrformet.2010.08.013, 2011. 12914, 12925
- Hanna, S. R.: Applications in Air Pollution Modeling, 1st edn., Springer, The Hague, the Netherlands, 275–310, doi:10.1007/978-94-010-9112-1\_7, 1982. 12919
- Heimann, M. and Reichstein, M.: Terrestrial ecosystem carbon dynamics and climate feedbacks, *Nature*, 451, 289–292, doi:10.1038/nature06591, 2008. 12913
- Henne, S., Brunner, D., Folini, D., Solberg, S., Klausen, J., and Buchmann, B.: Assessment of parameters describing representativeness of air quality in-situ measurement sites, *Atmos. Chem. Phys.*, 10, 3561–3581, doi:10.5194/acp-10-3561-2010, 2010. 12917
- Hiller, R. V., Bretscher, D., DelSontro, T., Diem, T., Eugster, W., Henneberger, R., Hobi, S., Hodson, E., Imer, D., Kreuzer, M., Künzle, T., Merbold, L., Niklaus, P. A., Rihm, B., Schellenberger, A., Schroth, M. H., Schubert, C. J., Siegrist, H., Stieger, J., Buchmann, N., and Brunner, D.: Anthropogenic and natural methane fluxes in Switzerland synthesized within a spatially explicit inventory, *Biogeosciences*, 11, 1941–1959, doi:10.5194/bg-11-1941-2014, 2014. 12915, 12917, 12929, 12933
- Kretschmer, R., Gerbig, C., Karstens, U., Biavati, G., Vermeulen, A., Vogel, F., Hammer, S., and Totsche, K. U.: Impact of optimized mixing heights on simulated regional atmospheric transport of CO<sub>2</sub>, *Atmos. Chem. Phys.*, 14, 7149–7172, doi:10.5194/acp-14-7149-2014, 2014. 12915
- Lauvaux, T., Schuh, A., Bocquet, M., and Wu, L.: Network design for mesoscale inversions of CO<sub>2</sub> sources and sinks, *Tellus B*, 1, 1–12, 2012. 12914
- Lawrence, D. M., Oleson, K. W., Flanner, M. G., Thornton, P. E., Sean, C., Lawrence, P. J., Zeng, X., Yang, Z.-L., Levis, S., Bonan, G. B., and Slater, A. G.: Parameterization improvements and functional and structural advances in version 4 of the Community Land Model, *Journal of Advances in Modeling Earth Systems*, 3, 1–29, doi:10.1029/2011MS00045, 2011. 12920
- Le Quéré, C., Takahashi, T., Buitenhuis, E. T., Rödenbeck, C., and Sutherland, S. C.: Impact of climate change and variability on the global oceanic sink of CO<sub>2</sub>, *Global Biogeochem. Cy.*, 24, GB4007, doi:10.1029/2009GB003599, 2010. 12913

|  |                              |
|--|------------------------------|
| <a href="#">Title Page</a>               |                              |
| <a href="#">Abstract</a>                 | <a href="#">Introduction</a> |
| <a href="#">Conclusions</a>              | <a href="#">References</a>   |
| <a href="#">Tables</a>                   | <a href="#">Figures</a>      |
| <a href="#">◀</a>                        | <a href="#">▶</a>            |
| <a href="#">◀</a>                        | <a href="#">▶</a>            |
| <a href="#">Back</a>                     | <a href="#">Close</a>        |
| <a href="#">Full Screen / Esc</a>        |                              |
| <a href="#">Printer-friendly Version</a> |                              |
| <a href="#">Interactive Discussion</a>   |                              |



Le Quéré, C., Andres, R. J., Boden, T., Conway, T., Houghton, R. A., House, J. I., Marland, G., Peters, G. P., Van Der Werf, G. R., Ahlström, A., Andrew, R. M., Bopp, L., Canadell, J. G., Ciais, P., Doney, S. C., Enright, C., Friedlingstein, P., Huntingford, C., Jain, A. K., Jourdain, C., Kato, E., Keeling, R. F., Klein Goldewijk, K., Levis, S., Levy, P., Lomas, M., Poulter, B., Rau-pach, M. R., Schwinger, J., Sitch, S., Stocker, B. D., Viovy, N., Zaehle, S., and Zeng, N.: The global carbon budget 1959–2011, *Earth Syst. Sci. Data*, 5, 165–185, doi:10.5194/essd-5-165-2013, 2013. 12913

MeteoSwiss: Klimabulletin Winter 2013/14, 1–6, MeteoSchweiz, Zuerich, available at: <http://www.meteoschweiz.admin.ch/content/dam/meteoswiss/de/Ungebundene-Seiten/Publikationen/Klimabulletin/doc/publi-klimabulletin-winter-20132014.pdf> (last access: 24 April 2015), 2014. 12926

Miles, N. L., Richardson, S. J., Davis, K. J., Lauvaux, T., Andrews, A. E., West, T. O., Banderu, V., and Crosson, E. R.: Large amplitude spatial and temporal gradients in atmospheric boundary layer CO<sub>2</sub> mole fractions detected with a tower-based network in the US upper Midwest, *J. Geophys. Res.*, 117, 1–13, doi:10.1029/2011JG001781, 2012. 12914

Pillai, D., Gerbig, C., Ahmadov, R., Rödenbeck, C., Kretschmer, R., Koch, T., Thompson, R., Neininger, B., and Lavrié, J. V.: High-resolution simulations of atmospheric CO<sub>2</sub> over complex terrain – representing the Ochsenkopf mountain tall tower, *Atmos. Chem. Phys.*, 11, 7445–7464, doi:10.5194/acp-11-7445-2011, 2011. 12915

Pillai, D., Gerbig, C., Kretschmer, R., Beck, V., Karstens, U., Neininger, B., and Heimann, M.: Comparing Lagrangian and Eulerian models for CO<sub>2</sub> transport – a step towards Bayesian inverse modeling using WRF/STILT-VPRM, *Atmos. Chem. Phys.*, 12, 8979–8991, doi:10.5194/acp-12-8979-2012, 2012. 12915

Rella, C. W., Chen, H., Andrews, A. E., Filges, A., Gerbig, C., Hatakka, J., Karion, A., Miles, N. L., Richardson, S. J., Steinbacher, M., Sweeney, C., Wastine, B., and Zellweger, C.: High accuracy measurements of dry mole fractions of carbon dioxide and methane in humid air, *Atmos. Meas. Tech.*, 6, 837–860, doi:10.5194/amt-6-837-2013, 2013. 12916

Ruckstuhl, A. F., Henne, S., Reimann, S., Steinbacher, M., Vollmer, M. K., O'Doherty, S., Buchmann, B., and Hueglin, C.: Robust extraction of baseline signal of atmospheric trace species using local regression, *Atmos. Meas. Tech.*, 5, 2613–2624, doi:10.5194/amt-5-2613-2012, 2012. 12917

|                                   |  |                              |
|-----------------------------------|--|------------------------------|
| <a href="#">Title Page</a>        | <a href="#">Abstract</a>                 | <a href="#">Introduction</a> |
| <a href="#">Conclusions</a>       | <a href="#">References</a>               |                              |
| <a href="#">Tables</a>            | <a href="#">Figures</a>                  |                              |
| <a href="#">◀</a>                 | <a href="#">▶</a>                        |                              |
| <a href="#">◀</a>                 | <a href="#">▶</a>                        |                              |
| <a href="#">Back</a>              | <a href="#">Close</a>                    |                              |
| <a href="#">Full Screen / Esc</a> |  |                              |
|                                   | <a href="#">Printer-friendly Version</a> |                              |
|                                   | <a href="#">Interactive Discussion</a>   |                              |



- Sarmiento, J. L., Gloor, M., Gruber, N., Beaulieu, C., Jacobson, A. R., Mikaloff Fletcher, S. E., Pacala, S., and Rodgers, K.: Trends and regional distributions of land and ocean carbon sinks, *Biogeosciences*, 7, 2351–2367, doi:10.5194/bg-7-2351-2010, 2010. 12913
- 5 Schibig, M. F., Steinbacher, M., Buchmann, B., van der Laan-Luijkx, I. T., van der Laan, S., Ranjan, S., and Leuenberger, M. C.: Comparison of continuous in situ CO<sub>2</sub> observations at Jungfraujoch using two different measurement techniques, *Atmos. Meas. Tech.*, 8, 57–68, doi:10.5194/amt-8-57-2015, 2015. 12917
- Schraff, C. H.: Mesoscale data assimilation and prediction of low stratus in the Alpine region, *Meteorol. Atmos. Phys.*, 64, 21–50, doi:10.1007/BF01044128, 1997. 12918
- 10 Seibert, P. and Frank, A.: Source-receptor matrix calculation with a Lagrangian particle dispersion model in backward mode, *Atmos. Chem. Phys.*, 4, 51–63, doi:10.5194/acp-4-51-2004, 2004. 12921
- Stephan, K., Klink, S., and Schraff, C.: Assimilation of radar-derived rain rates into the convective-scale model COSMO-DE at DWD, *Q. J. Roy. Meteor. Soc.*, 134, 1315–1326, doi:10.1002/qj.269, 2008. 12918
- 15 Stohl, A., Forster, C., Frank, A., Seibert, P., and Wotawa, G.: Technical note: The Lagrangian particle dispersion model FLEXPART version 6.2, *Atmos. Chem. Phys.*, 5, 2461–2474, doi:10.5194/acp-5-2461-2005, 2005. 12919
- Tans, P. P., Bakwin, P. S., and Guenther, D. W.: A feasible Global Carbon Cycle Observing System: a plan to decipher today's carbon cycle based on observations, *Glob. Change Biol.*, 2, 309–318, doi:10.1111/j.1365-2486.1996.tb00082.x, 1996. 12913
- 20 Tiedtke, M.: A comprehensive mass flux scheme for cumulus parameterization in large-scale models, *Mon. Weather Rev.*, 117, 1779–1800, 1989. 12919
- Vermeulen, A., Pieterse, G., Hensen, A., Schmidt, M., Ramonet, M., Messager, C., Jourd'Heuil, L., Manning, A., Gloor, M., Jordan, A., Popa, E., Thompson, R., Kozlova, E., Moors, E., Elbers, J., Jans, W., Ter Maat, H., Moncrieff, J., Conen, F., Haszpra, L., Barca, Z., Szilagyi, I., Stefani, P., Miglietta, F., and Lindroth, A.: CHIOTTO – Continuous High-Precision Tall Tower Observations of Greenhouse Gases, 1–118, available at: <http://www.ecn.nl/docs/library/report/2007/e07052.pdf> (last access: 24 April 2015), 2004. 12914
- 25 Vesala, T., Kljun, N., Rannik, U., Rinne, J., Sogachev, A., Markkanen, T., Sabelfeld, K., Foken, T., and Leclerc, M. Y.: Flux and concentration footprint modelling: state of the art., *Environ. Pollut.*, 152, 653–66, doi:10.1016/j.envpol.2007.06.070, 2008. 12915

|  |                              |
|--|------------------------------|
| <a href="#">Title Page</a>               |                              |
| <a href="#">Abstract</a>                 | <a href="#">Introduction</a> |
| <a href="#">Conclusions</a>              | <a href="#">References</a>   |
| <a href="#">Tables</a>                   | <a href="#">Figures</a>      |
| <a href="#">◀</a>                        | <a href="#">▶</a>            |
| <a href="#">◀</a>                        | <a href="#">▶</a>            |
| <a href="#">Back</a>                     | <a href="#">Close</a>        |
| <a href="#">Full Screen / Esc</a>        |                              |
| <a href="#">Printer-friendly Version</a> |                              |
| <a href="#">Interactive Discussion</a>   |                              |



[Title Page](#)

[Abstract](#)

[Introduction](#)

[Conclusions](#)

[References](#)

[Tables](#)

[Figures](#)

[◀](#)

[▶](#)

[◀](#)

[▶](#)

[Back](#)

[Close](#)

[Full Screen / Esc](#)

[Printer-friendly Version](#)

[Interactive Discussion](#)



**Table 1.** Details of the four measurement sites of the CarboCount CH network. From left to right, the site name, the site code, the measurement height(s), measured trace gases, the site altitudes (m a.s.l.), and the geographic site locations are listed.

| Site             | Code | Gases  | Device          | Height(s)            | Alt. | Lat., Lon.      |
|------------------|------|--|-----------------|----------------------|------|-----------------|
| Beromünster      | BEO  | CO <sub>2</sub> , CH <sub>4</sub> , CO, H <sub>2</sub> O | PICARRO G2401   | 212, 132, 72, 45, 12 | 797  | 47.1896, 8.1755 |
|                  |      | CO <sub>2</sub> , CH <sub>4</sub> , H <sub>2</sub> O     | PICARRO G2311-f |                      |      |                 |
| Früebüel         | FRU  | CO <sub>2</sub> , CH <sub>4</sub> , H <sub>2</sub> O     | PICARRO G2301   | 4                    | 982  | 47.1158, 8.5378 |
|                  |      | CO <sub>2</sub> , CH <sub>4</sub> , H <sub>2</sub> O     | PICARRO G2301   | 32                   | 443  | 47.0536, 7.2480 |
| Gimmiz           | GIM  | CO <sub>2</sub> , CH <sub>4</sub> , H <sub>2</sub> O     | PICARRO G2301   |                      |      |                 |
|                  |      | CO   | HORIBA APMA 360 |                      |      |                 |
| Lägern-Hochwacht | LAE  | CO <sub>2</sub> , CH <sub>4</sub> , CO, H <sub>2</sub> O | PICARRO G2401   | 32                   | 840  | 47.4822, 8.3973 |

- [Title Page](#)
- [Abstract](#) | [Introduction](#)
- [Conclusions](#) | [References](#)
- [Tables](#) | [Figures](#)
- | [◀](#) | [▶](#) |
- | [◀](#) | [▶](#) |
- [Back](#) | [Close](#)
- [Full Screen / Esc](#)
- [Printer-friendly Version](#)
- [Interactive Discussion](#)



**Table 2.** Simulation characteristics for the four measurement sites of the CarboCount CH network. Listed from left to right are FLEXPART-COSMO particle release heights (above model ground level), the “true” site altitudes (m a.s.l.), smoothed COSMO numerical weather prediction model’s ( $\sim 4 \text{ km}^2$ ) site altitude, and the geographic site locations.

| Site             | Meas. Height | Rel. Heights | Alt. | Alt. COSMO | Lat., Lon.      |
|------------------|--------------|--------------|------|------------|-----------------|
| Beromünster      | 212          | 212          | 797  | 723        | 47.1896, 8.1755 |
| Früebühl         | 5            | 50–100       | 982  | 813        | 47.1158, 8.5378 |
| Gimmiz           | 32           | 32           | 443  | 452        | 47.0536, 7.2480 |
| Lägern-Hochwacht | 32           | 100–200      | 840  | 566        | 47.4822, 8.3973 |

[Title Page](#)[Abstract](#) [Introduction](#)[Conclusions](#) [References](#)[Tables](#) [Figures](#)[◀](#) [▶](#)[◀](#) [▶](#)[Back](#) [Close](#)[Full Screen / Esc](#)[Printer-friendly Version](#)[Interactive Discussion](#)

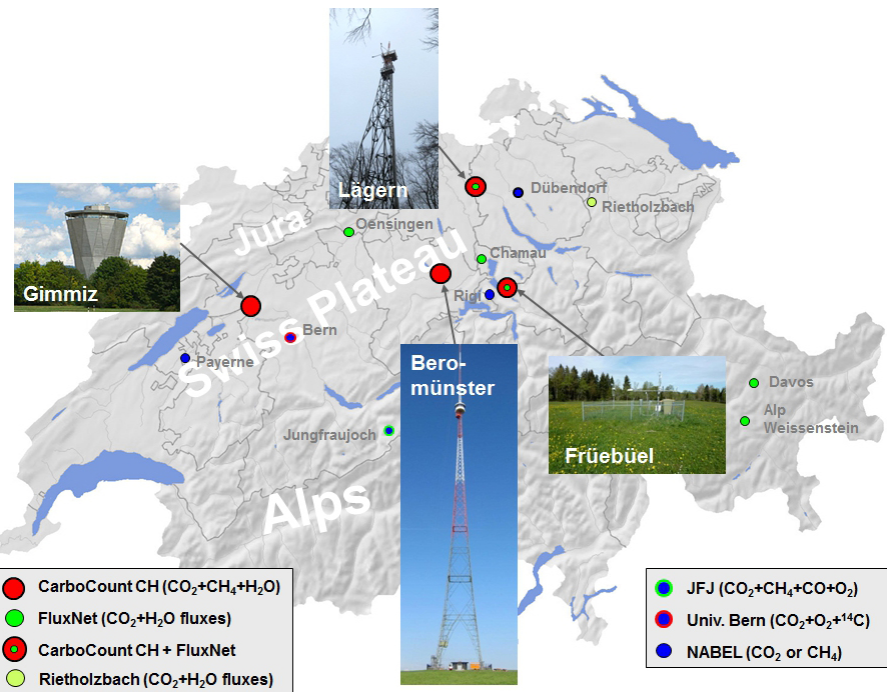


**Figure 1.** An overview of CarboCount CH measurement site locations within Switzerland: Beromünster (BEO), Früebühl (FRU), Gimmiz (GIM), and Lägern-Hochwacht (LAE). The sites are concentrated along the Swiss Plateau. The measurement heights and locations are listed in Table 1. Also shown are other sites with greenhouse gas concentration or flux measurements that complement the network. These include the sites of the Swiss Fluxnet, the high alpine research station Jungfraujoch, and sites of the Swiss air pollution monitoring network NABEL.

## Greenhouse gas observation network characterization

B. Ony et al.

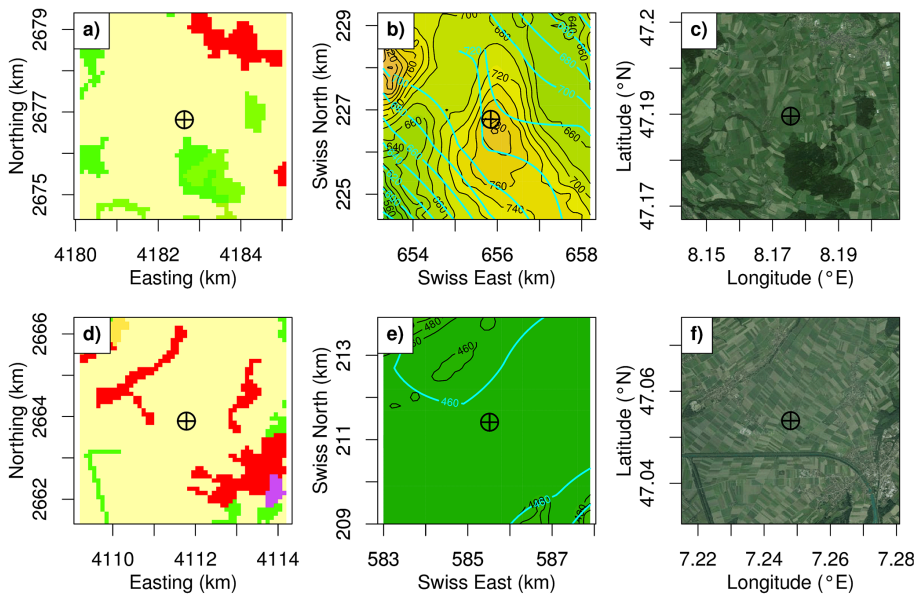


**Figure 2.** Site surroundings including land-use (first column), topography (second column), and Google aerial photo (third column), with Beromünster (**a–c**) in the first row, and Gimmiz (**d–f**) in the second row. The land-use (**a** and **d**) is based on CORINE 2006 land cover classes color-coded as follows – urban: red; food croplands: beige; evergreen forest: green; deciduous forest: light green; pasture: light brown; agro-forestry areas: tan. Cyan contour lines in the topography panels (**b** and **e**) denote the COSMO-2 model topography.

|  |                            |                              |
|--|----------------------------|------------------------------|
| <a href="#">Title Page</a>               | <a href="#">Abstract</a>   | <a href="#">Introduction</a> |
| <a href="#">Conclusions</a>              | <a href="#">References</a> |                              |
| <a href="#">Tables</a>                   | <a href="#">Figures</a>    |                              |
| <a href="#">◀</a>                        | <a href="#">▶</a>          |                              |
| <a href="#">◀</a>                        | <a href="#">▶</a>          |                              |
| <a href="#">Back</a>                     | <a href="#">Close</a>      |                              |
| <a href="#">Full Screen / Esc</a>        |                            |                              |
| <a href="#">Printer-friendly Version</a> |                            |                              |
| <a href="#">Interactive Discussion</a>   |                            |                              |



**Greenhouse gas  
observation network  
characterization**

B. Ony et al.

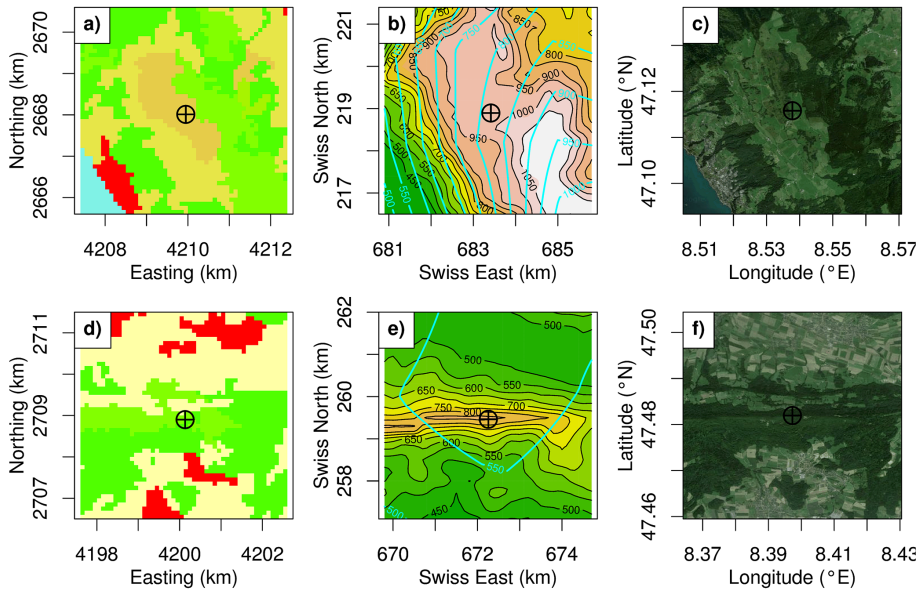


**Figure 3.** Similar to Fig. 2 with Früebüel (**a–c**) in the first row, and Lägern-Hochwacht (**d–f**) in the second row.

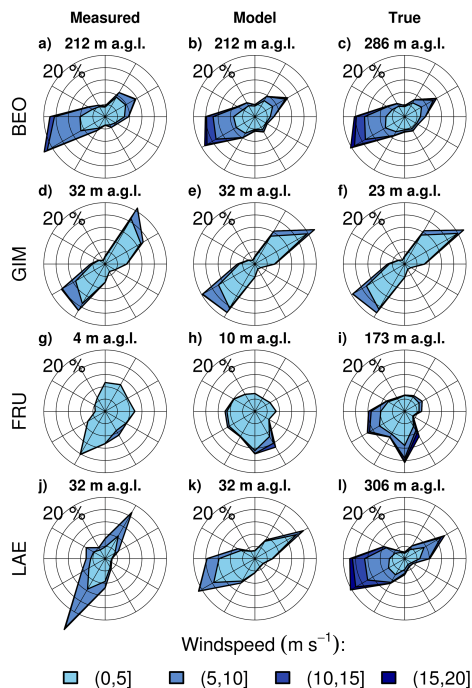


**Figure 4.** Wind roses at the four measurement sites during the study period (1 March 2013 to 28 February 2014) for observed (first column) and COSMO-2 simulated horizontal wind at two different model heights, at the height of the measurement a.m.g. (**Model**, second column), and at the true height of the measurement a.s.l. (**True**, third column). The wind roses display the windspeed probability distribution split into incident 30° wind direction bins. Wind from north is upward and circular lines demarcate graduating 5th percentiles. Labels above each panel show the height above ground for the measurements (first column), and height above COSMO-2 model ground for the simulated data (second and third columns).

## Greenhouse gas observation network characterization

B. Ony et al.

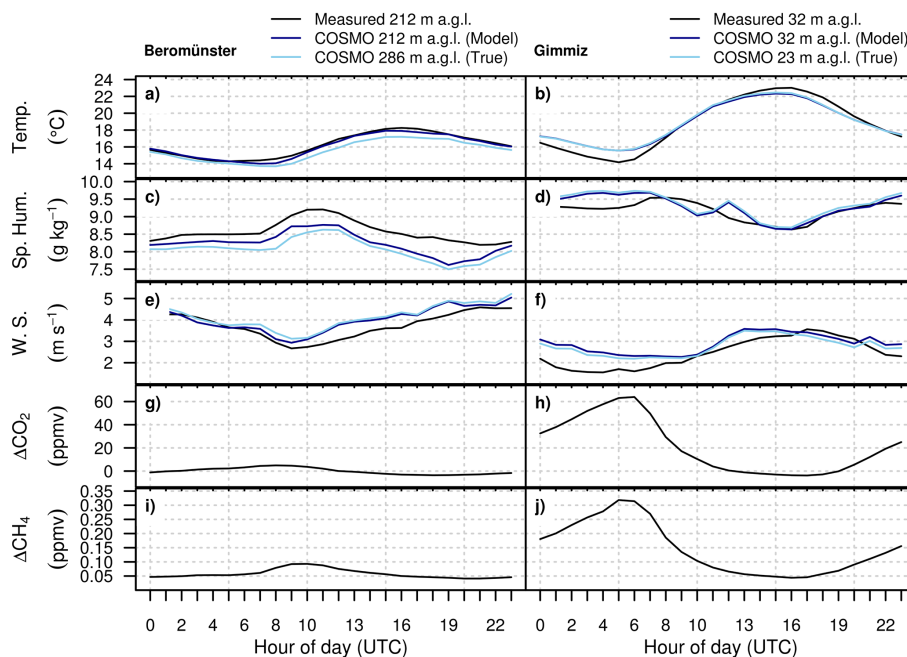


**Figure 5.** Mean summer (June–August 2013) diurnal cycle of measured and COSMO-2 simulated local meteorology at the sites Beromünster and Gimmiz: (a and b) temperature, (c and d) specific humidity (Sp. Hum.), and (e and f) windspeed (W. S.). Also shown are mean diurnal cycles of measured (g and h) regional  $\text{CO}_2$  signals ( $\Delta\text{CO}_2$ ), and (i and j) regional  $\text{CH}_4$  signals ( $\Delta\text{CH}_4$ ). The measurement and simulation heights above ground are listed in the figure legends. Simulated meteorology is shown for two different heights, the height of the measurement a.m.g. (**Model**, dark blue), and the simulation height a.m.g., which corresponds to the “true” measurement altitude a.s.l. (**True**, light blue). The time zone in Switzerland is Central European Time (CET or UTC+1).

[Title Page](#)

[Abstract](#)

[Introduction](#)

[Conclusions](#)

[References](#)

[Tables](#)

[Figures](#)

◀

▶

◀

▶

[Back](#)

[Close](#)

[Full Screen / Esc](#)

[Printer-friendly Version](#)

[Interactive Discussion](#)



## Greenhouse gas observation network characterization

B. Oney et al.

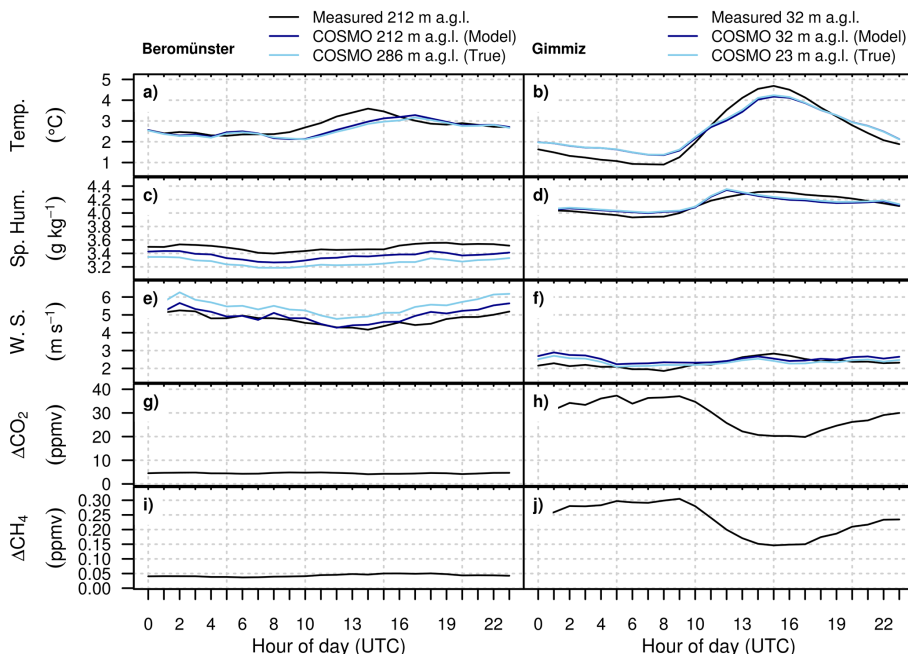


**Figure 6.** Similar to Fig. 5, the mean diurnal cycles during winter (December 2013–February 2014) at the sites Beromünster and Gimmiz.

# Greenhouse gas observation network characterization

B. Oney et al.

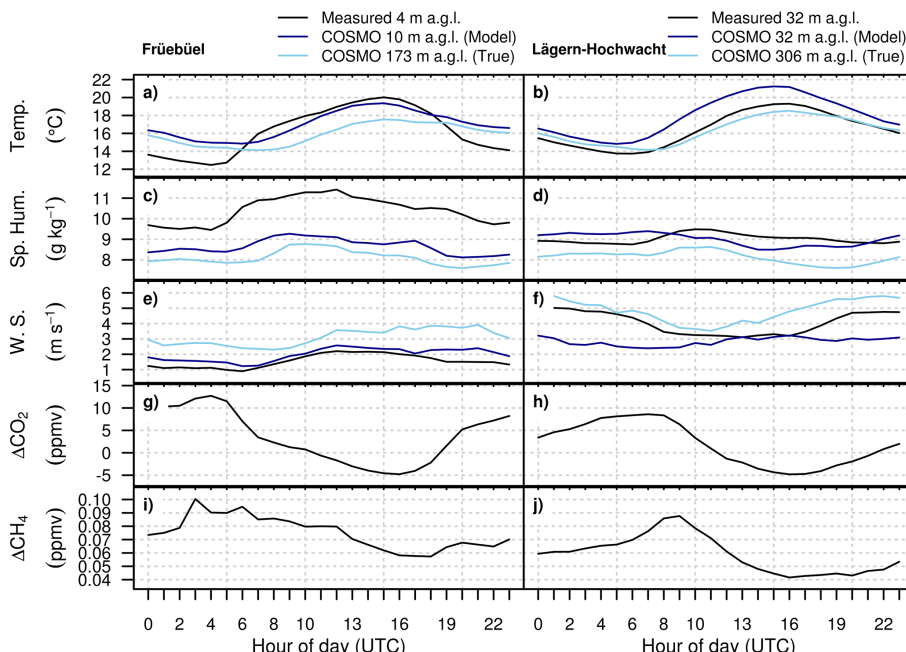


**Figure 7.** Similar to Fig. 5, the mean diurnal cycles during summer (June–August 2013) at the sites Früebüel and Lägern-Hochwacht. The Früebüel meteorological measurements were made at 2 m a.g.l.

Title Page

## Abstract

Introduction

## Conclusions

## References

## Table

## Figures



## Greenhouse gas observation network characterization

B. Oney et al.

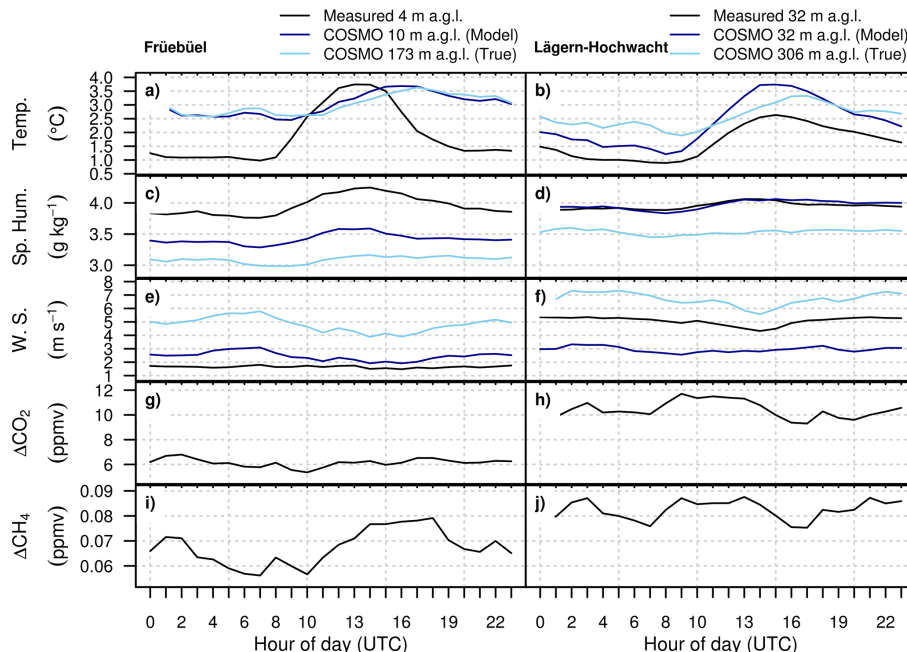


**Figure 8.** Similar to Fig. 5, mean diurnal cycles during winter (December 2013–February 2014) at the sites Fruebuel and Lagern-Hochwacht. The Fruebuel meteorological measurements were made at 2 m a.g.l.

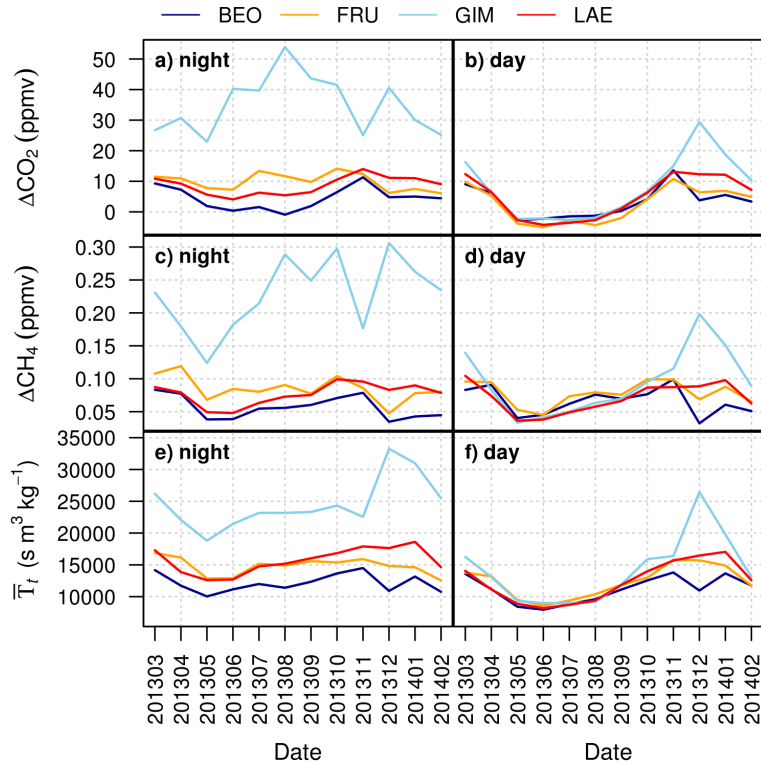


**Figure 9.** Monthly (YYYYMM) mean nighttime (00:00–03:00 UTC; **a**, **c**, and **e**) and daytime (12:00–15:00 UTC; **b**, **d**, and **f**) measured regional carbon dioxide signals,  $\Delta\text{CO}_2$ , measured regional methane signals,  $\Delta\text{CH}_4$ , and simulated monthly total surface sensitivities,  $T_t$  (Eq. 1), during the study's time period (1 March 2013 to 28 February 2014). Regional signals are computed as the measured concentration minus a background concentration estimate from Jungfraujoch, and total surface sensitivities provide a linear estimate of how much arriving air parcels at a measurement site have been in contact with the model domain's surface.

## Greenhouse gas observation network characterization

B. Ony et al.

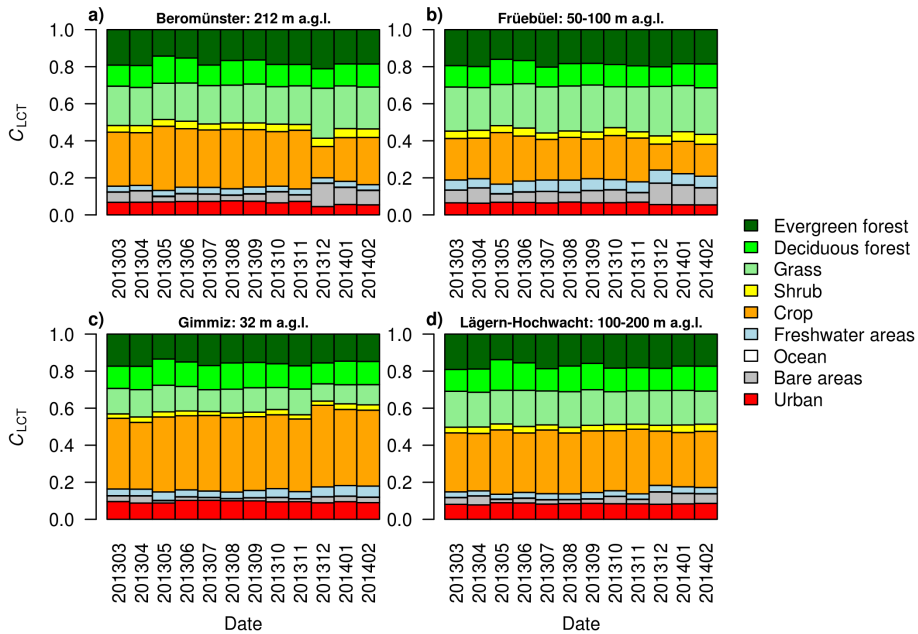


**Figure 10.** Monthly (YYYYMM) land cover type (LCT) contributions  $C_{\text{LCT}}$  (Eq. 2) for sites Beromünster **(a)**, Früebühl **(b)**, Gimmiz **(c)**, and Lägern-Hochwacht **(d)**, calculated as the pixel-wise multiplication of the monthly mean surface sensitivities with the respective LCT fraction and divided by the monthly averaged total surface sensitivities.

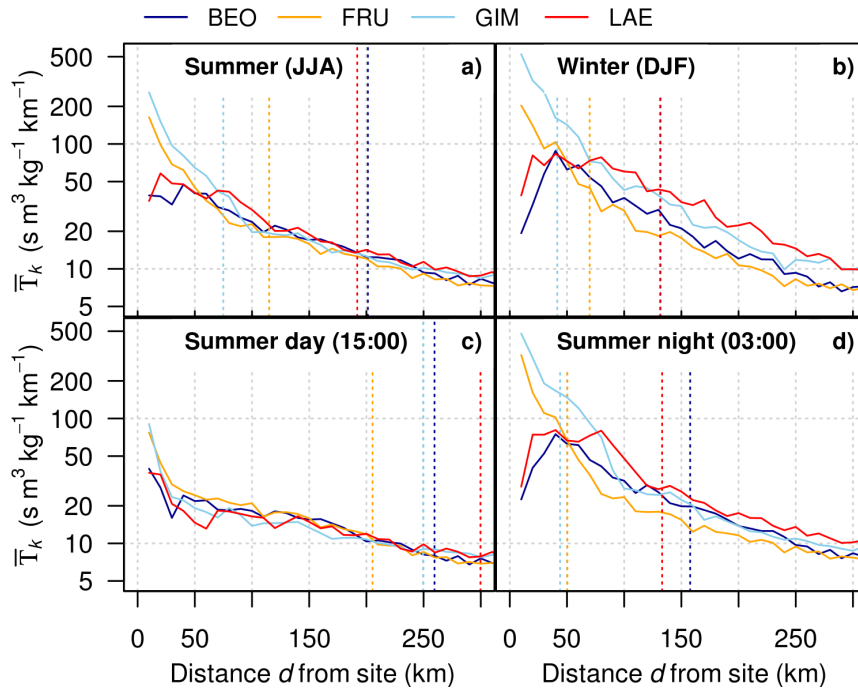


**Figure 11.** Surface sensitivities as a function of distance from the measurement site position  $\bar{T}_k$  (Eq. 3). Lines are color-coded according to measurement site (Beromünster: dark blue, Früebühl: orange, Gimmiz: light blue, Lägern-Hochwacht: red). The vertical dotted line is the radius at which the cumulative surface sensitivity starting from the measurement site's position reaches 50 % of the simulation domain total,  $\tau_{s50}$ . **(a)** Summer (June–August 2013), **(b)** winter (December 2013–February 2014), and **(c)** and **(d)** summer afternoon (15:00 UTC) and at nighttime (03:00 UTC), respectively. Please note the logarithmic y axis, and that during winter for Beromünster and Lägern-Hochwacht the 50 % vertical dotted lines overlap. The site-specific particle release heights are listed in Table 2. Local time is Central European Time (CET or UTC+1).

|  |                            |                              |
|--|----------------------------|------------------------------|
| <a href="#">Title Page</a>               | <a href="#">Abstract</a>   | <a href="#">Introduction</a> |
| <a href="#">Conclusions</a>              | <a href="#">References</a> |                              |
| <a href="#">Tables</a>                   | <a href="#">Figures</a>    |                              |
| <a href="#">◀</a>                        | <a href="#">▶</a>          |                              |
| <a href="#">◀</a>                        | <a href="#">▶</a>          |                              |
| <a href="#">Back</a>                     | <a href="#">Close</a>      |                              |
| <a href="#">Full Screen / Esc</a>        |                            |                              |
| <a href="#">Printer-friendly Version</a> |                            |                              |
| <a href="#">Interactive Discussion</a>   |                            |                              |

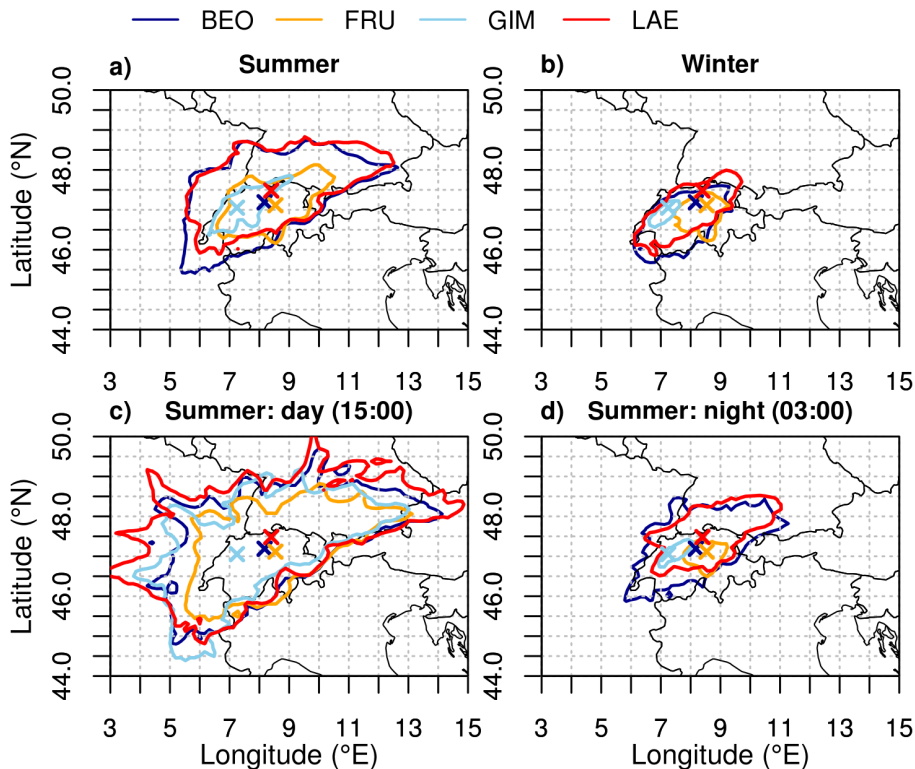


**Figure 12.** Area of surface influence (Eq. 5) defined as the isoline at the site-dependent value  $\tau_{s50}$  encompassing 50 % percent of the total mean surface sensitivities. Lines are color-coded according to measurement site—Beromünster: dark blue, Früebühl: orange, Gimmiz: light blue, Lägern-Hochwacht: red. **(a)** Summer (June–August, 2013), **(b)** winter (December 2013–February 2014), and **(c)** and **(d)** summer (June–August, 2013) in the afternoon (15:00 UTC) and at nighttime (03:00 UTC), respectively. Local time is Central European Time (CET or UTC+1).